MICROCOPY RESOLUTION TEST CHART

NATIONAL BUREAU OF STANDARDS-1963-A

AFAPL-TR-78-99

OPTICAL EMISSION FROM ION-ATOM AND ION-MOLECULE INTERACTIONS

E. GRANT JONES

WRIGHT STATE UNIVERSITY
BREHM LABORATORY
DAYTON, OHIO 45373

DECEMBER 1978

D D C

FEB 27 1979

B

AIR FORCE AERO PROPULSION LABORATORY
AIR FORCE WRIGHT AERONAUTICAL LABORATORIES
AIR FORCE SYSTEMS COMMAND
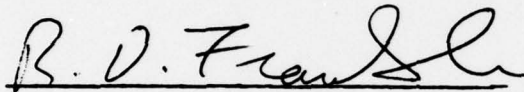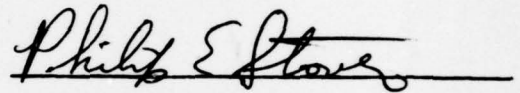WRIGHT-PATTERSON AIR FORCE BASE, OHIO 45433

79 02 21 061

UNCLASSIFIED
SECURITY CLASSIFICATION OF THIS PAGE (When Data Entered)

REPORT DOCUMENTATION PAGE	READ INSTRUCTIONS BEFORE COMPLETING FORM

1. REPORT NUMBER AFAPL-TR-78-99	2. GOVT ACCESSION NO.	3. RECIPIENT'S CATALOG NUMBER
4. TITLE (and Subtitle) Optical Emission from Ion-Atom and Ion Molecule Interactions		5. TYPE OF REPORT & PERIOD COVERED Final 1 July 1977-30 June 1978
		6. PERFORMING ORG. REPORT NUMBER 3699-L2 Final
7. AUTHOR(s) E. Grant Jones		8. CONTRACT OR GRANT NUMBER(s) Contract F33615-77-C-3141
9. PERFORMING ORGANIZATION NAME AND ADDRESS Wright State University Dayton, Ohio 45435		10. PROGRAM ELEMENT, PROJECT, TASK AREA & WORK UNIT NUMBERS 2301-S2-06
11. CONTROLLING OFFICE NAME AND ADDRESS Air Force Aero Propulsion Laboratory/POD-2 Air Force Systems Command Wright Patterson AFB. Ohio 45433		12. REPORT DATE December 1978
		13. NUMBER OF PAGES 84
14. MONITORING AGENCY NAME & ADDRESS(if different from Controlling Office)		15. SECURITY CLASS. (of this report) Unclassified
		15a. DECLASSIFICATION/DOWNGRADING SCHEDULE

16. DISTRIBUTION STATEMENT (of this Report)

Approved for public release; distirbution unlimited.

D D C
RECEIVED
FEB 27 1979
B

17. DISTRIBUTION STATEMENT (of the abstract entered in Block 20, if different from Report)

18. SUPPLEMENTARY NOTES

19. KEY WORDS (Continue on reverse side if necessary and identify by block number)

Ion-atom reactions, collisional excitation, charge-transfer reactions, rare-gas excitation, energy distribution in reaction products, translational-to-internal energy conversion, rare-gas potential curves, rare-gas molecular ions, xenon, krypton, argon.

20. ABSTRACT (Continue on reverse side if necessary and identify by block number)

Reactions of the rare gases, Rg, (Rg = Ar, Kr, Xe) with helium molecular ions, argon molecular ions and argon ions producing excitation have been investigated. All excitation is accompanied by the transfer of translational into internal energy via charge-transfer or collisional excitation reactions. Collisions of the argon atomic and molecular ions are efficient in exciting the resonant radiation in the RgI spectrum. Kinetic energy thresholds for several of these reactions are reported. — next page

DD FORM 1473 1 JAN 73   EDITION OF 1 NOV 65 IS OBSOLETE

20. Abstract (cont'd)

The symmetric system Xe ion/Xe has been studied with respect to production of Xe ion neutral atomic resonance radiation. The effects of the electronic state of the reacting xenon ions are discussed and possible reaction mechanisms are proposed.

FOREWORD

The present report, submitted December, 1978, and prepared by Dr. E. Grant Jones, outlines results obtained over the period 1 July 1977 - 30 June 1978 under the Air Force Aero Propulsion Laboratory, Project 2301, Task S2, Contract No. F33615-77-C-3141 with Wright State University, Brehm Laboratory, Dayton, OH, 45435. The Air Force project engineer was Captain Michael R. Stamm, AFAPL/POD-2.

The author would like to acknowledge Dr. Gary D. Sides, the support of the Brehm Laboratory Director, Dr. Thomas O. Tiernan, and helpful discussions with Dr. Alan Garscadden during the course of this study. In addition, the author thanks Mr. John G. Dryden for figure preparation and Mrs. Virginia Farley for typing the report. This study was sponsored by the Air Force Aero Propulsion Laboratory, Air Force Systems Command, United States Air Force, Wright-Patterson Air Force Base, Ohio, 45433. Subsequent publication of these results in Physical Review and Journal of Chemical Physics is planned with suitable acknowledgement given to the Air Force Aero Propulsion Laboratory.

TABLE OF CONTENTS

iv

LIST OF ILLUSTRATIONS

LIST OF TABLES

I. INTRODUCTION

Ion-neutral reactions play a significant role in determining the overall energy distribution in flames, discharges and the upper atmosphere.[1-3] Such reactions have been successfully studied for many years at the macroscopic level; however, recently as a result of the merging of ion-beam technology with optical spectroscopy, data at the microscopic level has been obtained. Reaction systems such as He^+/Xe which are nominally simple on the macroscopic scale[4] reveal a wealth of complexity when viewed at the microscopic level.[5-7] With state-to-state studies some understanding of the sophistication of quantum state preparation of the reactants and total energy dispersal in the products can be achieved. Recent ion-atom studies in the rare gas systems indicate a high degree of reaction specificity[5,7] in charge-transfer reactions. In molecular systems several lasers have been recently developed employing charge-transfer as the mechanism of laser excitation.[8-17] Most notable among these is the nitrogen-ion laser that is pumped by the charge-transfer reaction

$$He_2^+ + N_2 \rightarrow N_2^+ \; (B^2\Sigma_u^+) + 2He \tag{1}$$
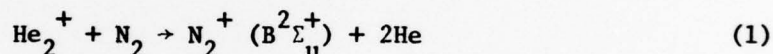
This reaction was first proposed as a pumping mechanism by Collins, Cunningham, Curry, Johnson and Stockton.[18] The first laser using this transition was reported by Collins, Cunningham and Stockton.[9] This laser was then scaled to higher power by Collins and Cunningham.[8] The pumping mechanism for this laser was also studied by Leventhal, Earl and Harris[19] who measured emission cross sections for He_2^+ on N_2 of 4×10^{-16} cm^2 for the $\Delta v = -1$ band of N_2^+ $(X^2\Sigma_g^+ \leftarrow B^2\Sigma_u^+)$ 8.5×10^{-16} cm^2 for the $\Delta v = 0$ band and 1×10^{-16} cm^2 for the $\Delta v = -2$ band. These transitions correspond to the lines, observed from the nitrogen ion laser, 391.4, 427.8 and 470.9 nm, respectively. The nitrogen ion laser has recently been operated in a discharge pumped mode at high powers (~ 0.5 MW pulses.)[20] This high power was obtained at 427.8 nm (0,1 band of $X^2\Sigma_g^+ \leftarrow B^2\Sigma_u^+$).

1

Waller, Collins and Cunningham[21] have recently observed stimulated emission from CO^+ pumped by charge-transfer from He_2^+. Maximum gain was observed for the 247.0 nm line corresponding to the (0,2) vibrational component of the $X^2\Sigma_1 \leftarrow B^2\Sigma$ transition. Leventhal and co-workers[22,23] have measured cross sections for excitation for He_2^+ on CO, NO, O_2 and CO_2 all with laser application potential.

A.   Description of the Apparatus

A schematic diagram of the light emission apparatus[24,25] is shown
in Figure 1. A single-focusing mass spectrometer, with a conventional
electron impact source, is used to produce a reactant ion beam, which is
mass resolved and ultimately directed into a collision chamber. The
mass resolution capability of the apparatus eliminates any uncertainty in
the identity of the reactant ions. The time required for the formation
of the reactant ion beam is long enough (> 10 μs) to allow the relaxation
to the ground state of any short-lived ionic species. The ion-source is
differentially pumped in order to reduce the scattering of the ion beam
during mass analysis. The relative intensity of the CH_5^+, CH_4^+ and CH_3^+
ions, produced from methane in the ion source, indicate a maximum source
pressure of about 50-100 millitorr. Baffle plates, located between the
ion source and the collision chamber, prevent most of the light produced
in the ion source from reaching the collision chamber and being collected
by the photon detection system. The mass-resolved ion beam is decelerated
to an energy in the range 2-1000 eV with an energy spread of 1 eV (FWHM).
The deceleration lens controls the energy of the reactant ions and focuses
the ion beam at the collision chamber entrance slit. The pressure in the
collision chamber is measured directly with an MKS Baratron gauge and is
generally less than 3 mtorr in order to reduce the importance of secondary
collision processes. The collision chamber is at room temperature. For
all the systems studied thus far, the observed photon signals have been
linear with respect to pressure below 10 mtorr, indicating that secondary
collisions are unimportant in the normal operation of the light emission
apparatus. No effects of resonance absorption have been observed.
The collision chamber ion exit slit is also the photon entrance slit of
a McPherson 1-meter monochromator. The monochromator is equipped with
a selection of gratings and photon detectors in order to permit a broad
spectral region (50-900 nm) to be monitored. The output from the photon
detectors is monitored by pulse counting techniques. The gratings and
detectors used in the present research are summarized in Tables 1 and 2,
respectively.

VACUUM U-V MONOCHROMATOR

PHOTO
MULTIPLIER

ION COLLECTOR

COLLISION CHAMBER
GAS INLET

DECELERATING
LENS

PULSE
AMPLIFIER

COUNTER

MAGNET
SECTOR

ION SOURCE

GAS INLET
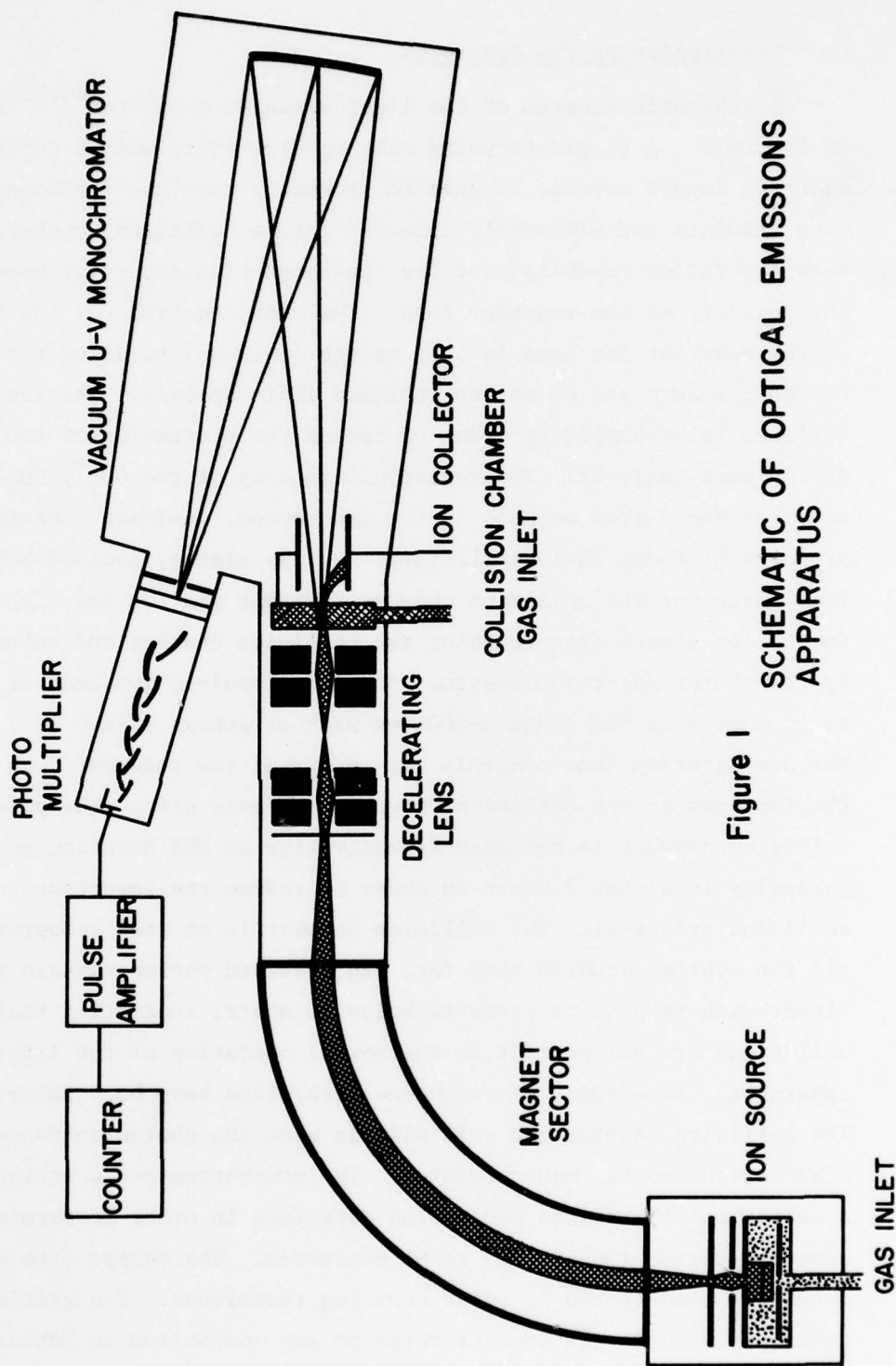
Figure I

SCHEMATIC OF OPTICAL EMISSIONS
APPARATUS

4

TABLE 1

GRATINGS USED IN THE CURRENT RESEARCH

Grating No.	Lines/mm	Blaze (nm)
1	600	200
2	600	90
3	1200	80
5	600	500

TABLE 2

DETECTORS USED IN THE CURRENT RESEARCH

Detector	Applicable Spectral Region (nm)
1. Channeltron	50-120
2. EMR (MgF$_2$ Window)	115-300
3. RCA C31034A	280-880

Typically $1-3 \times 10^{-8}$ A of any rare-gas ion can be transmitted through the collision chamber at 100 eV energy. One of the distinctive features of the first stage of the instrument is the high mass resolution for instruments of this type. For example, all of the Xe^+ isotopes (m/e 126, 127, 129, 130, 131, 132, 134 and 136) can be separated so that there is no ambiguity in separating isotopes for the heavy rare-gas systems.

An absolute calibration of the monochromator and photon detectors was made in the 450 to 900 nm spectral region, for each grating, using an NBS calibrated, tungsten strip lamp. Below 450 nm a relative calibration technique, based upon known grating reflectance and photon detector quantum efficiencies as a function of wavelength, was utilized. In addition, excellent agreement with absolute literature cross-sections for several reactions producing radiation in the visible and vacuum ultra-violet spectral region provides support for the validity of the calibration techniques. For example, a cross section of 0.60×10^{-16} cm^2 was measured in this laboratory for radiation arising from the ion-neutral collisions of He^+ on H_2.[26] This is in excellent agreement with a value of 0.51×10^{-16} cm^2 obtained by Dunn, Geballe and Pretzer.[27] This agreement illustrates that the calibration techniques used in the current research are valid and *that the in-line experimental arrangement used* in the present apparatus yields the same cross-sections as the perpendicular geometry used in the experiments of Dunn, Geballe and Pretzer.

B. Modifications

A recent increase in the first stage acceleration voltage from 300 to 1100 V has resulted in significant increase in the reactant ion currents. In Table 3 typical currents for the primary ions employed in this study are summarized. The lower limit for luminescence detection depends strongly on the primary ion current as well as collision chamber pressure, wavelength of radiation and type of grating and detector. The typical lower limit for a measurable cross section is 0.01×10^{-16} cm^2 and 0.3×10^{-16} cm^2 for reactions of atomic and molecular rare gas ions

6

respectively. Clearly there are distinct limitations in the reaction
sensitivity in studies of the molecular rare gas ions.

TABLE 3

PRIMARY ION CURRENTS FOR RARE GAS ATOMIC AND MOLECULAR IONS
OF 100 eV ENERGY USED IN THIS STUDY

Incident Ion	Ion Current (nA)
He^+	>30
$^{40}Ar^+$	>30
$^{84}Kr^+$	>20
$^{132}Xe^+$	>15
He_2^+	< 1
Ar_2^+	1

Introduction of ion deflection plates just before the collision
chamber entrance slit allows the use of a chop mode. With the deflection
plates off, light is collected from the collision chamber, deceleration lens
and background (ion-source). With the defection plates on, the ion beam
does not enter the collision chamber and light is collected from lens and
background sources only. The difference between these two signals, i.e.,
the net signal resulting from reactions occurring within the collision
chamber, is automatically displayed by the photon counter in the chop
mode.

C. Ion Formation

The atomic ions, He^+ and Ar^+ were formed by 70 V electron impact. For
the heavier rare-gases lower ionizing voltages were used to reduce the
percentage of metastables in the primary ion beam. The dimer ions He_2^+
and Ar_2^+ were formed at ionizing voltages < 25 V at ion-source pressures

7

in excess of 100 mtorr. The mechanism of molecular ion formation is the Hornbeck Molnar[28] associative ionization process (3)

$$Ar \xrightarrow{e^-} Ar^* + e^-$$ (2)

$$Ar^* + Ar \rightarrow Ar_2^+ + e^-$$ (3)

with negligible contribution from the three body process (4)

$$Ar^+ + 2Ar \rightarrow Ar_2^+ + Ar$$ (4)

D.   Discussion of Errors

Cross sections are measured with respect to two reference reactions[26,6]

$$He^+ + H_2 \rightarrow 121.6 \text{ nm} \quad H\ I(1s \leftarrow 2p)$$ (5)

$$He^+ + Xe \rightarrow 98.9 \text{ nm} \ XeII(5p^5 \ ^2P^o_{3/2} \leftarrow 6s \ ^4P_{1/2})$$ (6)
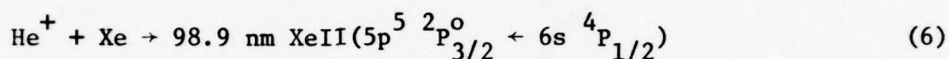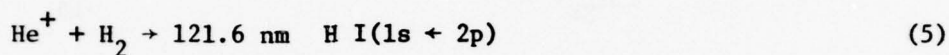
dpending on the spectral region. Over the region 121.6-150.0 nm no attempt was made to correct for variations in spectral response of the system. The quantum efficiency of the detector is flat in this interval that contains both the KrI and XeII resonance lines; however expected variations in grating reflectance would cause an overestimation of the intensities for the lines at longer wavelength. Over the shorter wavelength regions the quantum efficiency of the Channeltron and grating reflectance variation were taken into account to estimate the spectral response. Overall, cross sections are estimated to be accurate within a factor of five and the relative comparisons within a factor of two. Implicit in all calculations is that all radiation is emitted isotropically and without polarization.

The wavelength determinations are within ± 0.3 nm of the correct value. The errors in kinetic energy threshold determinations are estimated for each value. These are a function of the laboratory kinetic energy spread, center-of-mass conversion ratio, magnitude of the cross section, the counting statistics and finally, the nature of the threshold region.

8

III. RESULTS AND DISCUSSION

A. General

No evidence was found in this study for thermal reactions within the luminescence detection limits. As a result, most of the spectral scans and cross sections are measured for 100 eV ion impact. The results are arranged as follows

     B Reaction of He_2^+

     C Reaction of Ar_2^+

     D Miscellaneous ion-atom reactions

The recombination energies of the reactant ions are summarized in Table 4. The division between section B and C is related not only to the molecular ionic species, but also to the large gap in reactant ion recombination energy.

B. Reaction of He_2^+

1. Spectral Region 115-300 nm

The luminescence spectra for impact of He_2^+ at 100 eV impact on xenon and krypton are shown in Figure 2 and the lines are classified in Table 5. All of the lines observed have intensity at or below the detection limit for determining emission cross sections. Since the spectra are obtained operating in the continuous mode there is appreciable interference from lens and background contributions. These contributions cannot be satisfactorily eliminated by the pulse method because of the very low signal-to-noise ratio in the data. Line intensities are reported in Table 5 in terms of counts of radiation per second, per nA of ion signal per mtorr of collision gas, i.e., $cs^{-1} nA^{-1} mtorr^{-1}$. Most of the observed emissions can be classified as XeII or KrII by comparison with the spectral compilation of Striganov and Sventitskii.[32] The emitting ion levels are highly excited odd states formed via charge-transfer accompanied by extensive conversion of kinetic into internal energy. Because the intensities of the observed lines are near the detection limit, most of the emissions must be classified as having extensive contributions from

9

TABLE 4

PRIMARY IONS USED IN THIS STUDY AND THEIR RECOMBINATION ENERGY
(ground state ion-ground state neutral)

Incident Ion	Recombination Energy (eV)
He^+	24.58
He_2^+	18.3 - 20.3[a]
Ar^+	15.76[b] ($^2P^o_{3/2}$) 15.94[b] ($^2P^o_{1/2}$)
Ar_2^+	< 14.7[c,d]
Xe^+	12.13[b] ($^2P^o_{3/2}$) 13.44[b] ($^2P^o_{1/2}$)
Kr^+	14.00[b] ($^2P^o_{3/2}$) 14.67[b] ($^2P^o_{1/2}$)

---

[a]See Ref. 19.

[b]See Ref. 29.

[c]See Ref. 30.

[d]See Ref. 31.

10

Figure 2 a. Luminescence Spectrum Over Region 115-300 nm for 100 eV Impact of He_2^+ on Xenon. Ion current 0.68 nA, xenon pressure 1.5 mtorr, counting time 10 s, continuous mode.

Figure 2 b. Luminescence Spectrum Over the Region 115-300 nm for 100 eV Impact of He_2^+ on Krypton. Ion current 0.68 nA, krypton pressure 4 mtorr, counting time 10 s, continuous mode.

He_2^+ (100 eV) + Xe ⟶

He_2^+ (100 eV) + Kr ⟶

WAVELENGTH (nm)

300   270   240   210   180   150   120

11
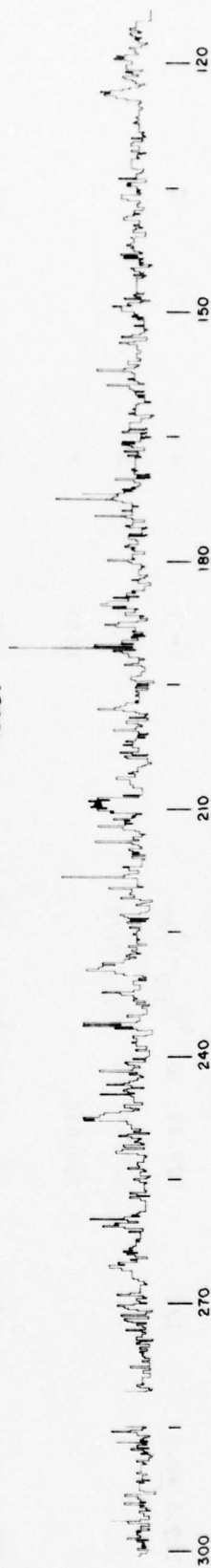
TABLE 5

He$_2^+$/Xe OBSERVED EMISSIONS

a. He$_2^+$/Xe Observed Emissions

Spectral Region: 115-300 nm

Kinetic Energy: 100 eV

Wavelength (nm)	Grating/ Detector	Classification Lower State	Upper State	Spectrum	Reference	Line Intensity[b] (cs^{-1} nA^{-1} mtorr^{-1})
229.4 ±0.2	1/2	229.24 5d $^4D_{5/2}$	$-^3 7^o_{7/2}$	XeII	a	< 2
		229.457 5d $^4D_{7/2}$	$-^3 7^o_{7/2}$	XeII	a	
		229.652	--	XeII	a	
231.6 ±0.2	1/2	231.37 5d $^4P_{5/2}$	$- 37^o_{5/2}$	XeII	a	< 2
		231.68 5d $^4D_{3/2}$	$-^7 7^o_{3/2}$	XeII	a	
247.6 ±0.2	1/2	247.018	--	XeII	a	< 2
		247.589	--	XeII	a	
		247.882	--	XeII	a	
248.8 ±0.2	1/2	248.911 5d $^4P_{3/2}$	$- 27^o_{5/2}$	XeII	a	< 2
		249.076 5d $^4P_{3/2}$	$- 25^o_{3/2}$	XeII	a	
		248.70 5p^5 $^2P^o_{1/2}$	$- 5p^6\, ^2S_{1/2}$	XeII	c (2nd order)	

12

TABLE 5 (concluded)

Wavelength (nm)	Grating/ Detector	Classification Lower State	Upper State	Spectrum	Reference	Line Intensity[b] $(cs^{-1}\ nA^{-1}\ mtorr^{-1})$
260.6 ±0.2	1/2	260.554	--		a	< 2
		260.693	--		a	
		260.752	$6s\ ^4P_{1/2}$ - $9^o_{3/2}$	XeII	a	

b. He_2^+/Kr Observed Emissions

Spectral Region: 115-300 nm
Kinetic Energy: 100 eV

123.8 ±0.2	1/2	--	--	--	--	< 0.5
172.9 ±0.2	1/2	--	--	--	--	< 0.5
197.3 ±0.2	1/2	--	--	--	--	< 0.5
208.7 ±0.2	1/2	208.673	$4d\ ^4D_{7/2}$ - $5f\ ^4F^o_{7/2}$	KrII	a	< 0.5
		208.816	$4d\ ^4D_{7/2}$ - $5f\ ^4F^o_{9/2}$	KrII	a	
228.8 ±0.2	1/2	228.779	$5s'\ ^2D_{5/2}$ - $6^o_{7/2}$	KrII	a	< 0.5
246.6 ±0.2	1/2	246.477	$4d\ ^4F_{7/2}$ - $2^o_{7/2}$	KrII	a	< 0.5
264.6 ±0.2	1/2	264.306	$4d\ ^4P_{3/2}$ - $5f\ ^4D^o_{3/2}$	KrII	a	< 0.5

[a] See Ref. 32.
[b] All lines associated with higher kinetic energy processes occuring in lens.
[c] See Ref. 6.

collisions within the deceleration lens at kinetic energies within the range 0.1-1 keV.

Significantly from Table 5 all the line classifications are consistent with charge-transfer excitation analogous to He^{+} reactions.[5-7] The XeI and KrI resonant lines which fall in the observed spectral region are noticeably absent.

The He_2^+/Xe system was also studied at 10 eV impact. Two lines at 124.5 and 248.9 nm corresponding to the XeII transition $5p^5\ ^2P^o_{1/2} \leftarrow 5p^6\ ^2S_{1/2}$ in the first and second order were observed. Pressure dependence indicated bimolecular excitation. Counting the 124.5 nm line using the pulse mode indicated no contribution from reaction in the collision chamber confirming the above conclusions that the observed emissions arise from higher energy processes occurring within the deceleration lens.

The He[+]/H_2 excitation of Lyman-alpha emission, reaction (5), is used both for wavelength and cross section calibration.[26] During calibration, the analogous reaction He_2^+/H_2 was studied under pulse conditions to compare the reaction cross section. A cross section of $0.06 \times 10^{-16}\ cm^2$ was measured for reaction (7) at 100 eV impact for Lyman-alpha production.

$$He_2^+ + H_2 \xrightarrow{100\ eV} (He_2H)^+ + H^*(\text{Lyman-alpha}) \qquad (7)$$
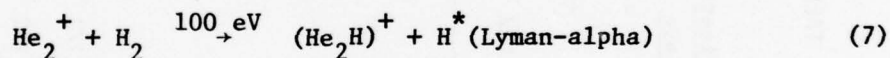
This is one-tenth the value obtained for the He^{+}/H_2 reaction.[26]

2. Spectral Region 55-125 nm

The luminescence spectra for impact of He_2^+ at 100 eV impact on xenon and krypton are shown in Figures 3 and 4, respectively, and the observed lines are classified in Tables 6 and 7. In the reaction with xenon all lines can be classified in XeII corresponding to the charge-transfer reaction (8)

$$He_2^+ + Xe \rightarrow (He_2) + Xe^+ \qquad (8)$$

14

He$_2^+$ (100eV) + Xe →

x10

WAVELENGTH (nm)

105   90   75   60
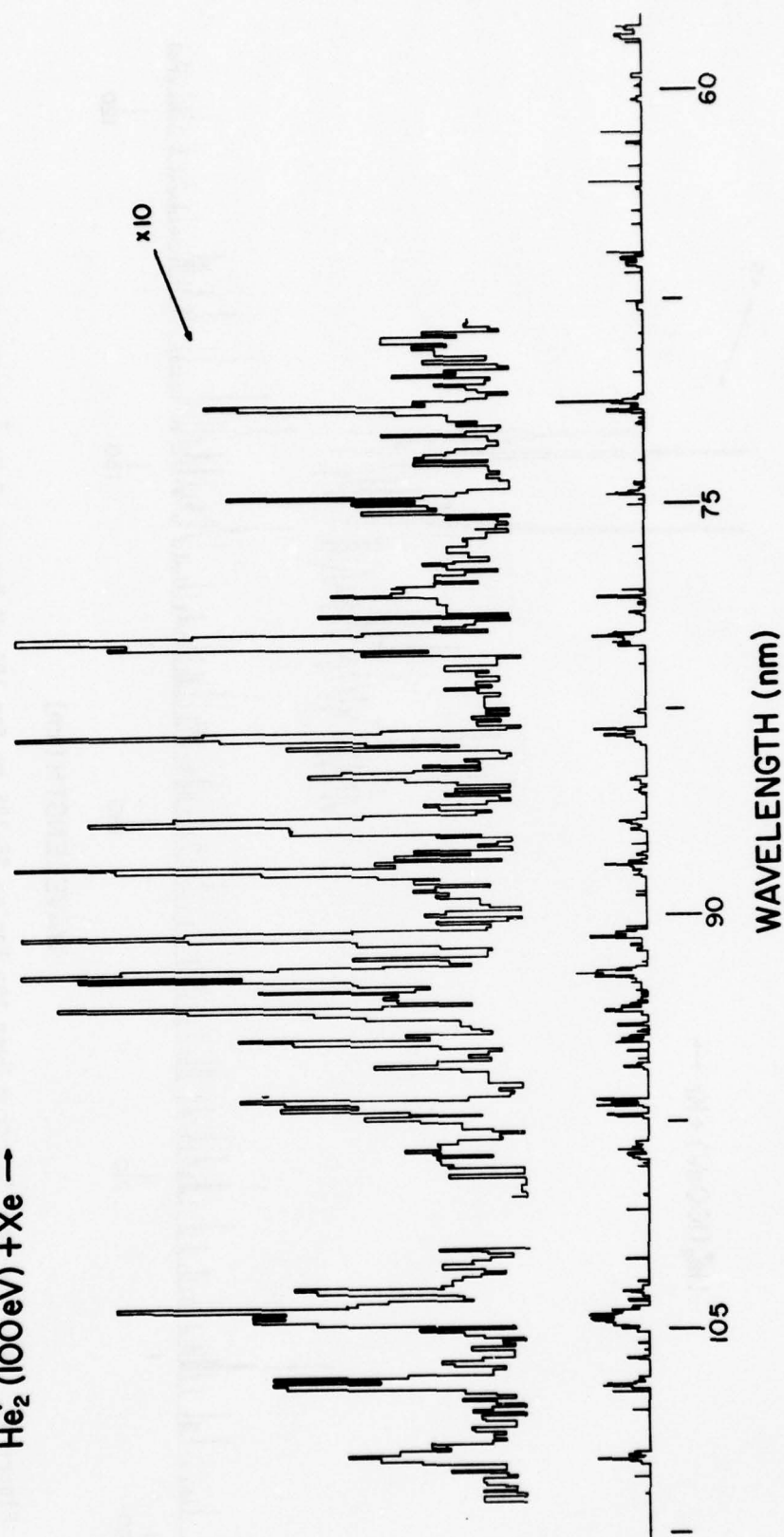
Figure 3. Luminescence Spectrum Over the Region 57.5–120 nm for 100 eV Impact of He$_2^+$ on Xenon. Ion current 0.6 nA, xenon pressure 4 mtorr, counting time 5 s lower trace, 25 s upper trace, upper trace sensitivity X10, continuous mode.
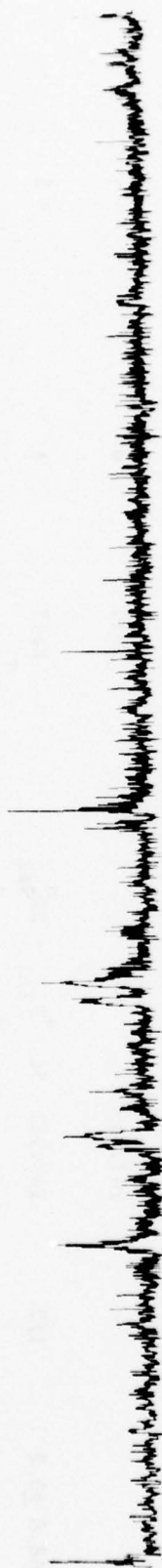
15

He$_2^+$(100eV) + Kr →

×5

WAVELENGTH (nm)
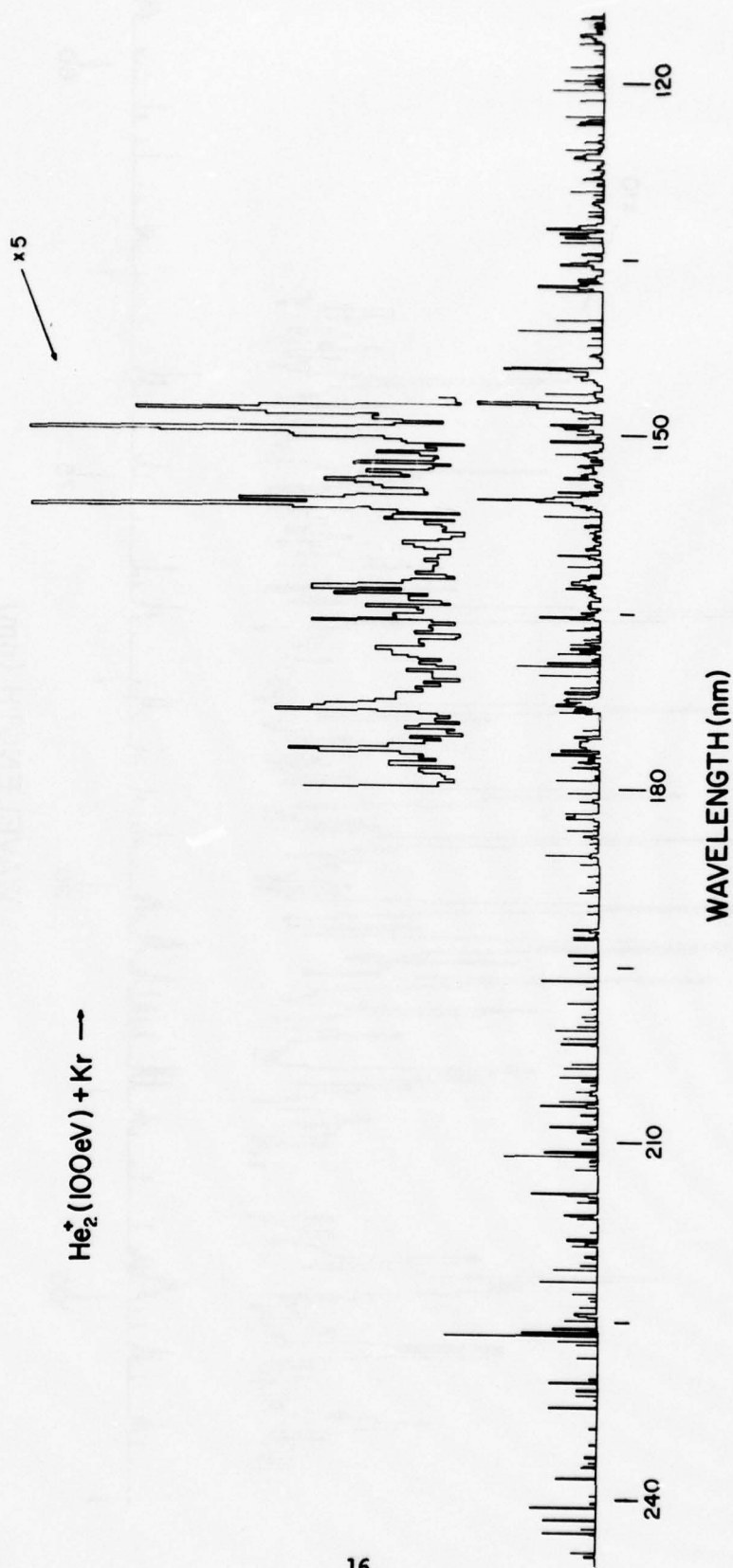
Figure 4. Luminescence Spectrum Over the Region 55-125 nm for 100 eV Impact of He$_2^+$ on Krypton. Ion current 0.54 nA, krypton pressure 3 mtorr, counting time 5 s lower trace, 25 s upper trace, upper trace sensitivity X5, continuous mode.

16

TABLE 6

He_2^+/Xe OBSERVED EMISSIONS

Spectral Region: 57.5-120 nm
Kinetic Energy: 100 eV

Wavelength (nm)	Grating/ Detector	Classification Lower State	Upper State	Spectrum	Reference	Line Intensity (cs^{-1} nA^{-1} $mtorr^{-1}$)	Cross Section (10^{-18} cm^2)
66.5 ±0.3	3/1					<0.1	
71.64 ±0.3	3/1	$5p^5\ ^2P^o_{3/2}$	$6d\ ^4F_{5/2}$	XeII	a	<0.1	
		$5p^5\ ^2P^o_{3/2}$	$6d\ ^4F_{3/2}$	XeII	a		
		$5p^5\ ^2P^o_{3/2}$	$20_{1/2}$	XeII	a		
		$5p^5\ ^2P^o_{3/2}$	$7s'\ ^2D_{3/2}$	XeII	a		
75.05 ±0.3	3/1	$5p^5\ ^2P^o_{3/2}$	$7s\ ^4P_{5/2}$	XeII	a	<0.1	
		$5p^5\ ^2P^o_{3/2}$	$7s\ ^4P_{3/2}$	XeII	a		
		$5p^5\ ^2P^o_{3/2}$	$2_{1/2}$	XeII	a		
		$5p^5\ ^2P^o_{3/2}$	$4_{1/2}$	XeII	a		
		$5p^5\ ^2P^o_{3/2}$	$4_{3/2}$	XeII	a		
		$5p^5\ ^2P^o_{1/2}$	$6d\ ^4P_{3/2}$	XeII	a		

TABLE 6 (continued)

Wavelength (nm)	Grating/ Detector	Classification Lower State	Upper State	Spectrum	Reference	Line Intensity (cs^{-1} nA^{-1} $mtorr^{-1}$)	Cross Section (10^{-18} cm^2)
80.3 $\pm$0.3	3/1	$5p^5$ $^2P^o_{3/2}$	$5d''$ $^2D_{3/2}$	XeII	a	0.3	4(6)[b]
		$5p^5$ $^2P^o_{3/2}$	$6s''$ $^2S_{1/2}$	XeII	a		
83.75 $\pm$0.3	3/1	$5p^5$ $^2P^o_{3/2}$	$5d''$ $^2D_{5/2}$	XeII	a	0.3	3(5)[b]
86.94 $\pm$0.3	3/1	$5p^5$ $^2P^o_{3/2}$	$5d'$ $^2F_{5/2}$	XeII	a	0.1	
91.06 $\pm$0.3	3/1	$5p^5$ $^2P^o_{3/2}$	$5d$ $^2D_{5/2}$	XeII	a	0.3	4(9.5)[b]
92.56 $\pm$0.3	3/1	$5p^5$ $^2P^o_{3/2}$	$5d$ $^2D_{3/2}$	XeII	a	0.2	3(15.5)[b]
		$5p^5$ $^2P^o_{3/2}$	$6s'$ $^2D_{5/2}$	XeII	a		
93.84 $\pm$0.3	3/1	$5p^5$ $^2P^o_{3/2}$	$5d$ $^4P_{1/2}$	XeII	a	<0.1	
		$5p^5$ $^2P^o_{3/2}$	$5d$ $^4P_{5/2}$	XeII	a		
94.81 $\pm$0.3	3/1	$5p^5$ $^2P^o_{3/2}$	$5d$ $^2P_{3/2}$	XeII	a	<0.1	
97.21 $\pm$0.3	3/1	$5p^5$ $^2P^o_{3/2}$	$6s$ $^2P_{3/2}$	XeII	a	<0.1	
98.75 $\pm$0.3	3/1	$5p^5$ $^2P^o_{3/2}$	$6s$ $^4P_{1/2}$	XeII	a	<0.1	

18

TABLE 6 (concluded)

Wavelength (nm)	Grating/ Detector	Classification Lower State	Upper State	Spectrum	Reference	Line Intensity $(cs^{-1}\ nA^{-1}\ mtorr^{-1})$	Cross Section $(10^{-18}\ cm^2)$
104.94 ±0.3	3/1	$5p^5\ ^2P^o_{3/2}$	$5d\ ^4D_{5/2}$	XeII	a	0.3	$6(25.3)^b$
		$5p^5\ ^2P^o_{1/2}$	$5d\ ^2P_{1/2}$	XeII	a		
		$5p^5\ ^2P^o_{3/2}$	$6s\ ^4P_{3/2}$	XeII	a		
107.38 ±0.3	3/1	$5p^5\ ^2P^o_{3/2}$	$6s\ ^4P_{5/2}$	XeII	a	<0.1	
110.08 ±0.3	3/1	$5p^5\ ^2P^o_{3/2}$	$5p^6\ ^2S_{1/2}$	XeII	a	0.1	$2(16.5)^b$

[a] See Ref. 6.

[b] Values in parentheses refer to He$^+$/Xe reaction. See Ref. 6.

19

TABLE 7

He$_2^+$/Kr OBSERVED EMISSIONS

Spectral Region: 55.0–120 nm
Kinetic Energy: 100 eV

Wavelength (nm)	Grating/ Detector	Classification Lower State	Upper State	Spectrum	Reference	Line Intensity (cs^{-1} nA^{-1} mtorr^{-1})	Cross Section (10^{-18} cm^2)
58.38 ±0.3	3/1	4p^5 ^{2}P$^o_{3/2}$	(^{1}D)6s ^{2}D$_{5/2}$	KrII	a	< 0.1	
		4p^5 ^{2}P$^o_{3/2}$	(^{1}D)6s ^{2}D$_{3/2}$	KrII	a		
		4p^5 ^{2}P$^o_{1/2}$	(^{3}P)7s ^{4}P$_{1/2}$	KrII	a		
		4p^5 ^{2}P$^o_{1/2}$	(^{1}D)5d ^{2}P$_{3/2}$	KrII	a		
		4p^5 ^{2}P$^o_{1/2}$	(^{3}P)7s ^{2}P$_{3/2}$	KrII	a		
		4p^5 ^{2}P$^o_{1/2}$	(^{1}D)5d ^{2}P$_{1/2}$	KrII	a		
				HeI	b		
63.44 ±0.3	3/1	4p^5 ^{2}P$^o_{3/2}$	(^{3}P)6s ^{4}P$_{5/2}$	KrII	a	< 0.1	
		4p^5 ^{2}P$^o_{3/2}$	(^{3}P)6s ^{4}P$_{3/2}$	KrII	a		
		4p^5 ^{2}P$^o_{1/2}$	(^{3}P)6s ^{2}P$_{1/2}$	KrII	a		
		4p^5 ^{2}P$^o_{1/2}$	(^{3}P)5d ^{4}D$_{1/2}$	KrII	a		
66.55 ±0.3	3/1	4p^5 ^{2}P$^o_{3/2}$	(^{1}D)4d ^{2}D$_{5/2}$	KrII	a	< 0.1	
68.01 ±0.3	3/1	4p^5 ^{2}P$^o_{3/2}$	(^{1}S)5s ^{2}S$_{1/2}$	KrII	a	< 0.1	
		4p^5 ^{2}P$^o_{1/2}$	(^{1}D)4d ^{2}P$_{3/2}$	KrII	a		
		4p^5 ^{2}P$^o_{1/2}$	(^{1}D)4d ^{2}P$_{1/2}$	KrII	a		

TABLE 7 (continued)

Wavelength (nm)	Grating/ Detector	Classification		Spectrum	Reference	Line Intensity ($cs^{-1}\ nA^{-1}\ mtorr^{-1}$)	Cross Section ($10^{-18}\ cm^2$)
		Lower State	Upper State				
69.03 ±0.3	3/1	$4p^5\ ^2P^o_{1/2}$	$(^1D)4d\ ^2D_{3/2}$	KrII	a	< 0.1	
72.74 ±0.3	3/1	$4p^5\ ^2P^o_{3/2}$	$(^3P)4d\ ^2D_{5/2}$	KrII	a	< 0.1	
74.13 ±0.3	3/1	$4p^5\ ^2P^o_{3/2}$	$(^3P)4d\ ^4P_{5/2}$	KrII	a	0.22	2(1.0)[c]
		$4p^5\ ^2P^o_{3/2}$	$(^3P)4d\ ^2D_{3/2}$	KrII	a		
75.18 ±0.3	3/1	$4p^5\ ^2P^o_{3/2}$	$(^3P)4d\ ^4P_{3/2}$	KrII	a	0.44	4(1.4)[c]
		$4p^5\ ^2P^o_{3/2}$	$(^3P)4d\ ^2F_{5/2}$	KrII	a		
77.31 ±0.3	3/1	$4p^5\ ^2P^o_{3/2}$	$(^3P)4d\ ^4F_{5/2}$	KrII	a	< 0.1	
		$4p^5\ ^2P^o_{1/2}$	$(^3P)4d\ ^2D_{3/2}$	KrII	a		
78.10 ±0.3	3/1	$4p^5\ ^2P^o_{3/2}$	$(^1D)5s\ ^2D_{5/2}$	KrII	a	1.2	12(3.7)[c]
81.81 ±0.3	3/1	$4p^5\ ^2P^o_{1/2}$	$(^1D)5s\ ^2D_{3/2}$	KrII	a	< 0.1	
84.44 ±0.3	3/1	$4p^5\ ^2P^o_{3/2}$	$(^3P)5s\ ^2P_{3/2}$	KrII	a	< 0.1	

21

TABLE 7 (concluded)

Wavelength (nm)	Grating/ Detector	Classification		Spectrum	Reference	Line Intensity (cs⁻¹ nA⁻¹ mtorr⁻¹)	Cross Section (10^{-18} cm²)
		Lower State	Upper State				
86.73 ±0.3	3/1	$4p^5\,^2P^o_{1/2}$	$(^3P)5s\,^2P_{1/2}$	KrII	a	0.1	
		$4p^5\,^2P^o_{1/2}$	$(^3P)4d\,^4D_{3/2}$	KrII	a		
		$4p^5\,^2P^o_{3/2}$	$(^3P)5s\,^4P_{3/2}$	KrII	a		
88.56 ±0.3	3/1	$4p^5\,^2P^o_{3/2}$	$(^3P)5s\,^4P_{5/2}$	KrII	a	0.49	6(2.8)[c]

[a]See Ref. 6.

[b]See Ref. 29.

[c]Values in parentheses refer to He⁺/Kr reaction. See Ref. 6.

22

All observed processes are endothermic requiring the transfer of in excess of 3 eV of translational into internal energy. As was observed at the longer wavelengths, the cross sections for excitation are small. The emission cross sections for the major lines are shown in the last column of Table 6. For comparison, emission cross sections for the He^+/Xe system are given in parentheses.[6] For the major lines, the emission cross sections from reaction of He_2^+ and He^+ compare favorably. The overall total emission cross section is estimated as $< 0.5 \times 10^{-16}$ cm^2; this is about five times smaller than that for He^+/Xe reactions. This may be related to the difference in recombination energies of the reactant ions (see Table 4) and the corresponding difference in reaction endothermicity. Typical of charge-transfer spectra, there is a high degree of specificity in the populated states, but significantly, there is no evidence for the selective production of Xe^+ in $J = 1/2$ states as has been observed in the He^+/Xe system.[7]

For the reaction system He_2^+/Kr all of the observed emission lines can be classified in the KrII spectrum. All excitation occurs via the endothermic charge-transfer reaction (9)

$$He_2^+ + Kr \rightarrow (He_2) + Kr^+ \tag{9}$$

The emission cross sections listed in the last column of Table 7 are in each case at least a factor of two larger than those given in parentheses for the corresponding He^+/Kr reaction. The estimate of $< 0.5 \times 10^{-16}$ cm^2 for the overall emission cross section indicates that He_2^+ and He^+ are about equally efficient in producing emission lines in the KrII spectrum.[33]

The kinetic energy variation of the 78.1 nm KrII line classified as $4p^5 \, ^2P^o_{3/2} \leftarrow (^1D) \, 5s \, ^2D_{5/2}$ is shown in Figure 5. The signal-to-noise ratio is too low in this data to observe any fine structure or determine an accurate threshold. The cross section remains approximately constant from 100 eV down to 30 eV impact, then drops rapidly to zero characteristic of an endothermic reaction.

23
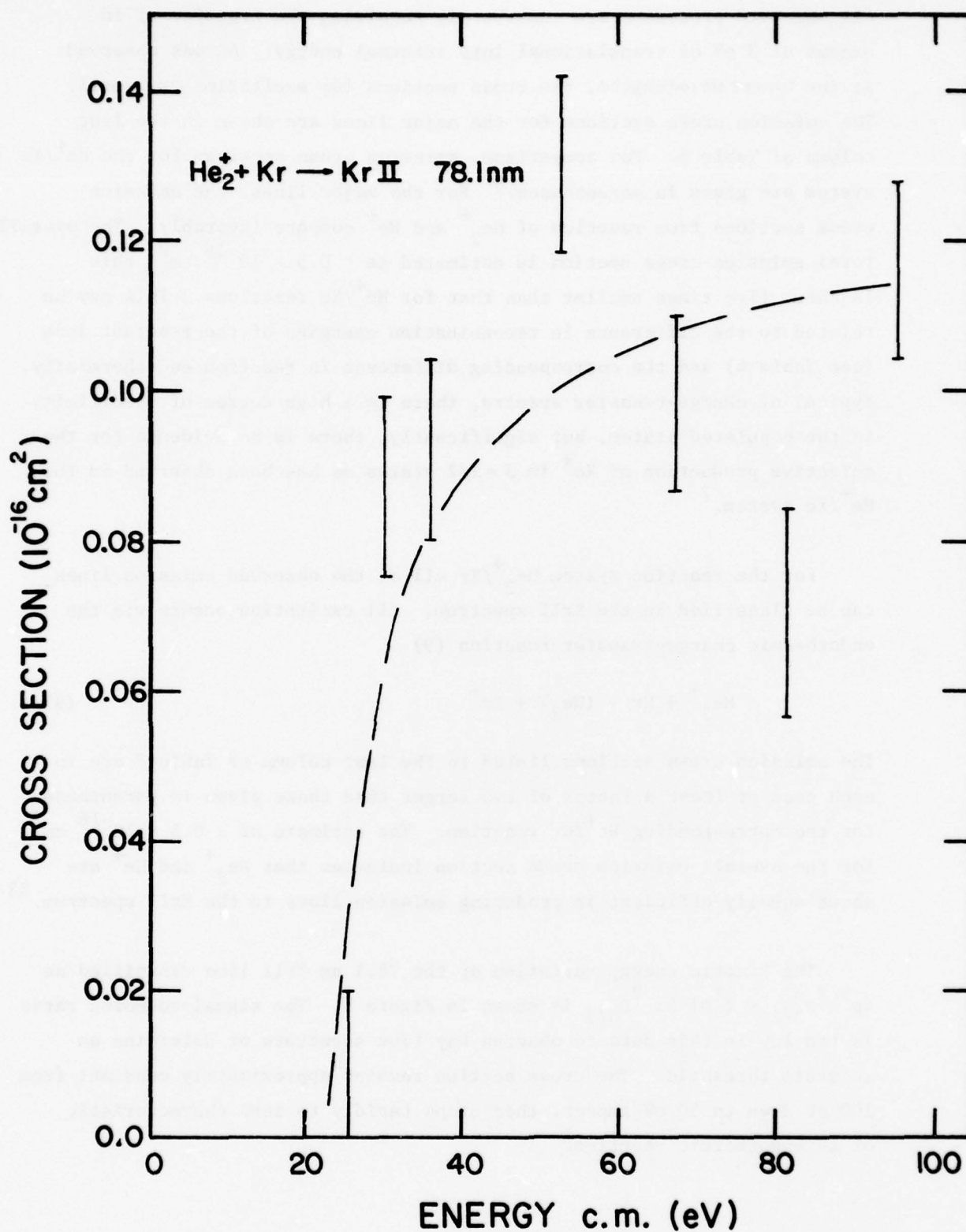
Figure 5. Kinetic Energy Variation of 78.1 nm Kr iI line $4p^5\ ^2P^0_{3/2} \leftarrow (^1D)5s\ ^2D_{5/2}$ for He_2^+/Kr reaction.

24

Table 8 briefly summarizes the comparison of He_2^+ and He^+ reactions with xenon and krypton. In addition the following points can be made.

- all observed reactions occur via endothermic charge-transfer to produce excited ion states of the target gas.

- all observed reactions involve the transfer of translational energy into internal energy

- all emission lines have cross sections $\leq 10^{-17}$ cm^2

- He^+ is more efficient than He_2^+ in producing XeII excitation in collisions with xenon

- He^+ and He_2^+ are about equally efficient in producing KrII excitation in collisions with krypton

- some selectivity is observed in the excited products in the charge-transfer reactions but there is no evidence for the preferential production of states with $J = 1/2$ as has been reported for He^+ reactions[7]

- no evidence is found for collisional excitation of the projectile ion or the target atom; i.e., the emission cross section for HeI, KrI, or XeI lines is less than 10^{-18} cm^2

TABLE 8

SUMMARY OF RESULTS OF He^+, He_2^+ COLLISIONS WITH

XENON AND KRYPTON FOR 100 eV IMPACT

	He^+		He_2^+	
Collision Gas	Excitation	Emission Cross Section (10^{-16} cm^2)	Excitation	Emission Cross Section (10^{-16} cm^2)
Xenon	XeII	2.5	XeII	< 0.5
Krypton	KrII	0.3	KrII	< 0.5

C. Reaction of Ar_2^+

1. Ar_2^+/Xe

The observed luminescence over the spectral region 55-300 nm produced in 100 eV Ar_2^+/Xe collisions is shown in Figures 6-8. The observed lines

25
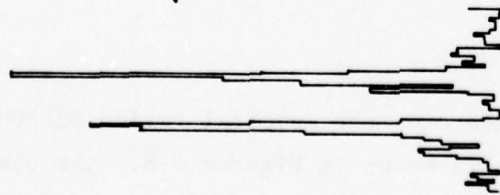
Figure 6. Luminescence Spectrum Over the Region 55-110 nm for 100 eV Impact of Ar_2^+ on Xenon. Ion current 1.2 nA, xenon pressure 4 mtorr, counting time 5s lower trace, 25 s upper trace, upper trace sensitivity X5, continuous mode.

$Ar_2^+(100\,eV) + Xe \rightarrow$

120

150

180

210

WAVELENGTH (nm)
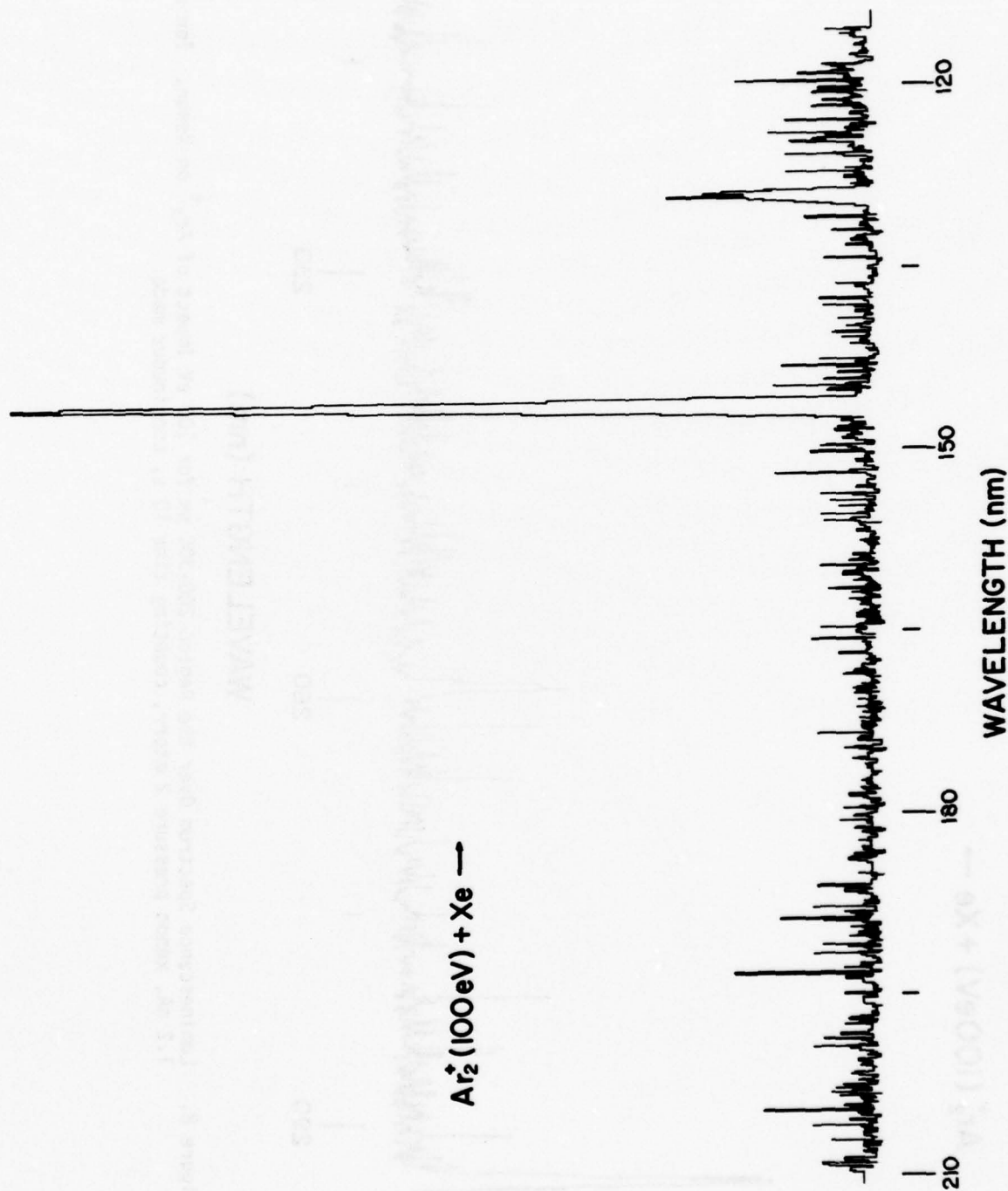
Figure 7. Luminescence Spectrum Over the Region 115-210 nm for 100 eV Impact of Ar_2^+ on Xenon. Ion current 1.2 nA, xenon pressure 2 mtorr, counting time 10 s, continuous mode.

27

Ar$_2^+$ (100eV) + Xe →

WAVELENGTH (nm)
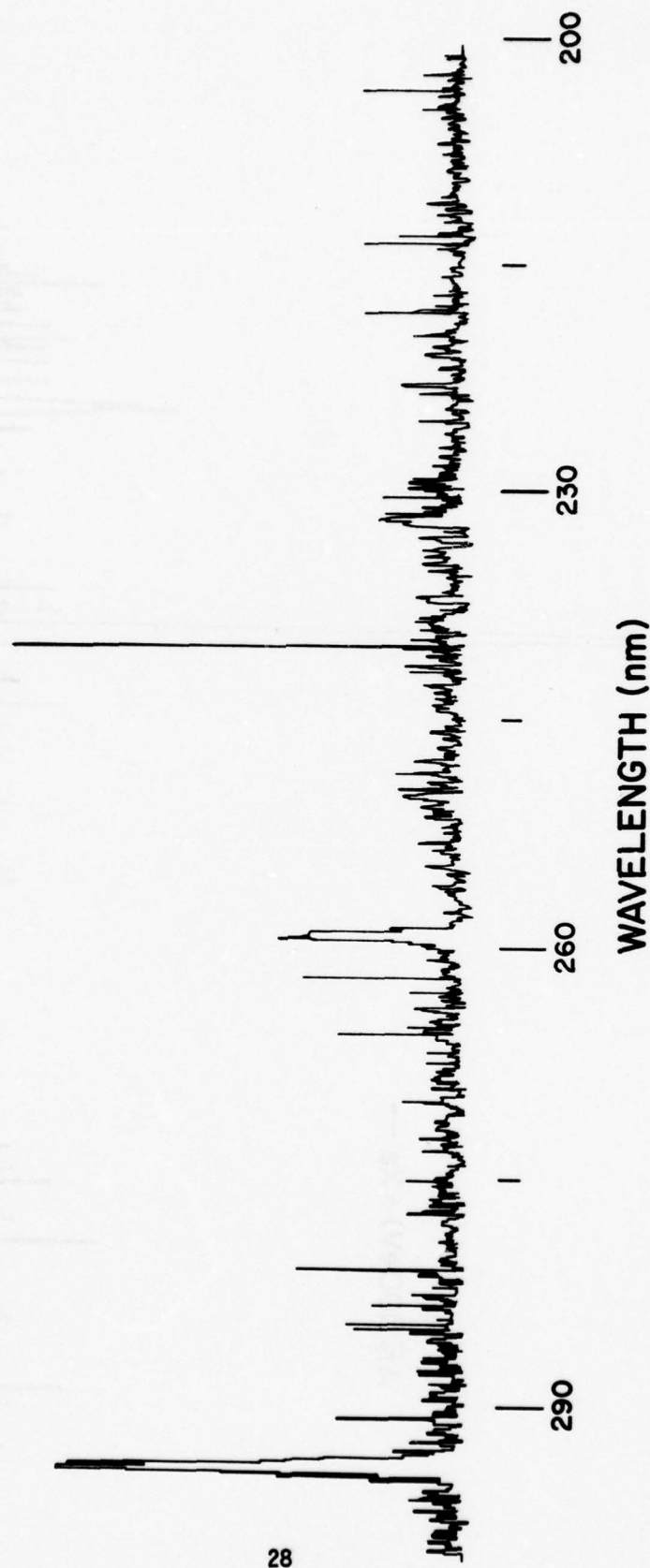
Figure 8. Luminescence Spectrum Over the Region 200-300 nm for 100 eV Impact of Ar$_2^+$ on Xenon. Ion current 1.2 nA, xenon pressure 2 mtorr, counting time 10 s, continuous mode.

28

are summarized in Table 9 along with the spectral classifications and emission cross sections determined using the pulsing mode. Basically the only lines observed with measurable emission cross sections are the two lowest resonance lines of ArI and XeI. There is no evidence for any other excited atom states. The XeI lines classified[34] as $3p^6\ ^1S_0 \leftarrow 6s\ [3/2]_1^o$ and $3p^6\ ^1S_0 \leftarrow 6s'\ [1/2]_1^o$ correspond to emissions from the lowest possible energy states produced in the collisional excitation reaction (10).

$$Ar_2^+ + Xe \rightarrow Ar_2^+ + Xe^* \tag{10}$$

Reaction (10) is endothermic by 8.43 and 9.57 eV for the $6s\ [3/2]_1^o$ and $6s'\ [1/2]_1^o$ states, respectively. The metastable states with $J = 2,0$ cannot be detected because of their long lifetimes

The ArI resonance lines can be produced in the charge-transfer reaction (11).

$$Ar_2^+ + Xe \rightarrow Ar + Ar^* + Xe^+ \tag{11}$$

Depending on the recombination energy range for Ar_2^+ and the states of Ar^* and Xe^+, reaction (11) is endothermic by at least 9.3 eV. A second reaction is possible involving a collision induced dissociation (12)

$$Ar_2^+ + Xe \rightarrow Ar^+ + Ar^* + Xe \tag{12}$$
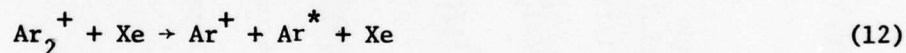
Production of the 106.6 nm ArI line is endothermic by at least 13 eV.

Thus, formation of Xe* $6s\ [3/2]_1^o$ via reaction (10) thermochemically requires the least amount of kinetic energy transfer and occurs with the largest observed cross section. The emission cross sections for Xe* $6s'\ [1/2]_1^o$, Ar* $6s\ [3/2]_1^o$, $6s'\ [1/2]_1^o$ at 100 eV impact are almost an order of magnitude smaller.

The kinetic energy behavior of three of these lines is shown in Figure 9. Figure 9 indicates that the ArI and XeI lines are produced in the present experiments via endothermic reactions involving large

TABLE 9

Ar$_2^+$/Xe OBSERVED EMISSIONS

Spectral Region: 55–300 nm
Kinetic Energy: 100 eV

Wavelength (nm)	Grating/ Detector	Classification Lower State	Upper State	Spectrum	Reference	Line Intensity (cs⁻¹ nA⁻¹ mtorr⁻¹)	Cross Section (10⁻¹⁶ cm²)
104.69 ±0.3	3/1	$3p^6\,{}^1S_0$	$4s'[1/2]^o_1$	ArI	a	0.3	0.06
106.56 ±0.3	3/1	$3p^6\,{}^1S_0$	$4s[3/2]^o_1$	ArI	a	0.2	0.04
107.47 ±0.3	3/1	$5p^5\,{}^2P^o_{3/2}$	$6s\,{}^4P_{5/2}$	XeII	b	< 0.1	~0.1
129.4 ±0.3	1/2	$5p^6\,{}^1S_0$	$6s'[1/2]^o_1$	XeI	a	0.9	~0.1
146.6 ±0.3	1/2	$5p^6\,{}^1S_0$	$6s[3/2]^o_1$	XeI	a	6.0	~0.7
259.2 ±0.2	1/2	Second Order 129.6 nm		XeI	a	--	~0.8
294.2 ±0.2	1/2	Second Order 147.1 nm		XeI	a	6.7	~0.8

aSee Ref. 32

bSee Ref. 6
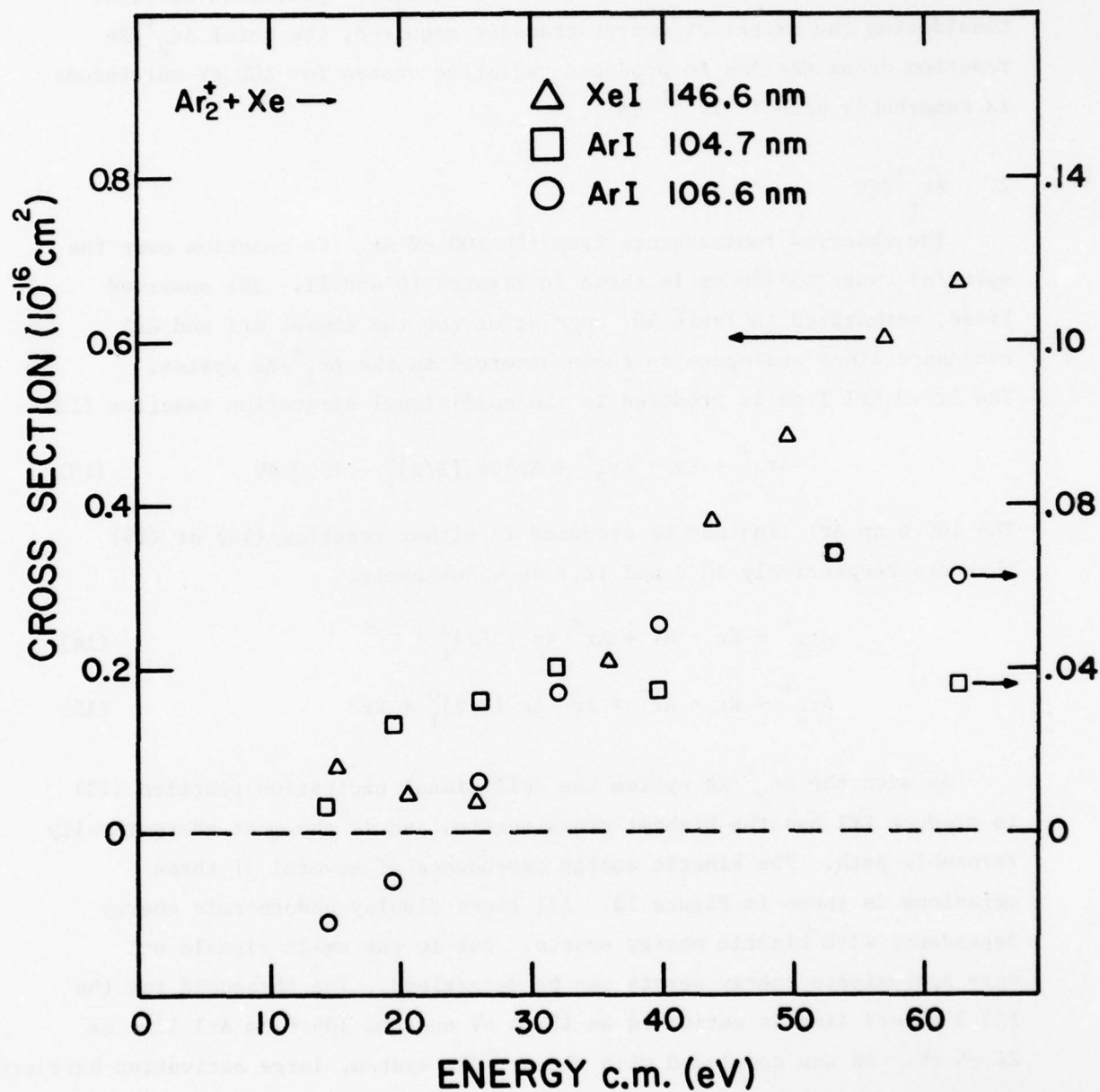
Figure 9. Kinetic Energy Dependence of Emission Cross Section for 146.6 nm XeI,
104.7 nm and 106.6 nm ArI lines in Ar_2^+/Xe Collisions.

kinetic energy barriers. The onset for the 146.6 nm XeI line is estimated as 25 $\pm$3 eV, and the ArI lines estimated as 20 $\pm$10 eV.

Formation of the major Xe* emitting state 6s $[3/2]_1^o$ requires the transfer of considerably more kinetic into internal energy than is thermochemically required. This reaction must proceed via a surface crossing high on the steep repulsive portion of the $(Ar_2Xe)^+$ potential surface. Considering the extent of energy transfer required, the total Ar_2^+/Xe reaction cross section to produced radiative states for 100 eV collisions is remarkably high ($\sim 10^{-16}$ cm^2).

2. Ar_2^+/Kr

The observed luminescence from the 100 eV Ar_2^+/Kr reaction over the spectral range 55-250 nm is shown in Figures 10 and 11. The observed lines, summarized in Table 10, consist of the two lowest ArI and KrI resonance lines analogous to those observed in the Ar_2^+/Xe system. The 123.3 KrI line is produced in the collisional excitation reaction (13)

$$Ar_2^+ + Kr \rightarrow Ar_2^+ + Kr^*5s \ [3/2]_1^o - 10.0 \ eV \qquad (13)$$
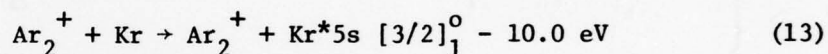
The 106.6 nm ArI line may be produced in either reaction (14) or (15) that are respectively 10.9 and 12.7 eV endothermic.

$$Ar_2^+ + Kr \rightarrow Ar + Ar^* \ 4s \ [3/2]_1^o + Kr^+ \qquad (14)$$

$$Ar_2^+ + Kr \rightarrow Ar^+ + Ar^* \ 4s \ [3/2]_1^o + Kr \qquad (15)$$
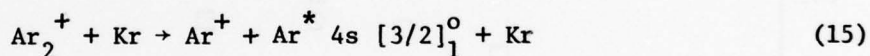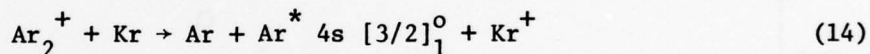
As with the Ar_2^+/Xe system the collisional excitation reaction (13) to produce KrI has the highest cross section and is the most energetically favorable path. The kinetic energy dependence of several of these emissions is shown in Figure 12. All lines display endothermic energy dependence with kinetic energy onsets. Due to the small signals only very approximate energy onsets can be determined. The threshold for the 123.3 nm KrI line is estimated as 18 $\pm$5 eV and the 106.6 nm ArI line as 24 $\pm$5 eV. As was concluded with the Ar_2^+/Xe system, large activation barriers exceeding the endothermicity are indicated for reactions (13)-(15).
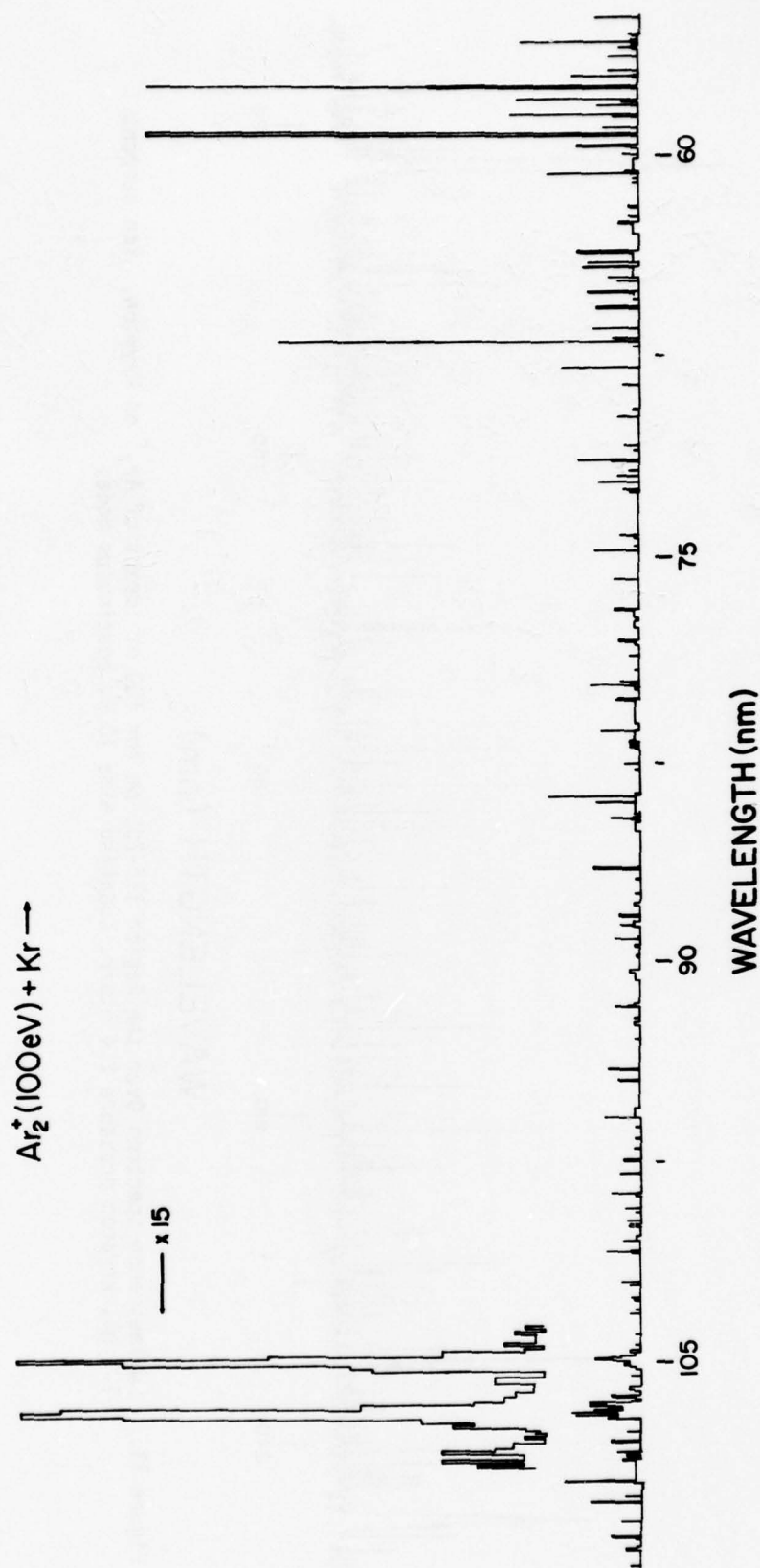
Ar_2^+(100eV) + Kr →

Figure 12. Luminescence Spectrum Over the Region 55-110 nm for 100 eV Impact of Ar_2^+ on Krypton. Ion current 0.9 nA, krypton pressure 3 mtorr, counting time 5 s, continuous mode.

33

$Ar_2^+ (100\ eV) + Kr \longrightarrow$

WAVELENGTH (nm)
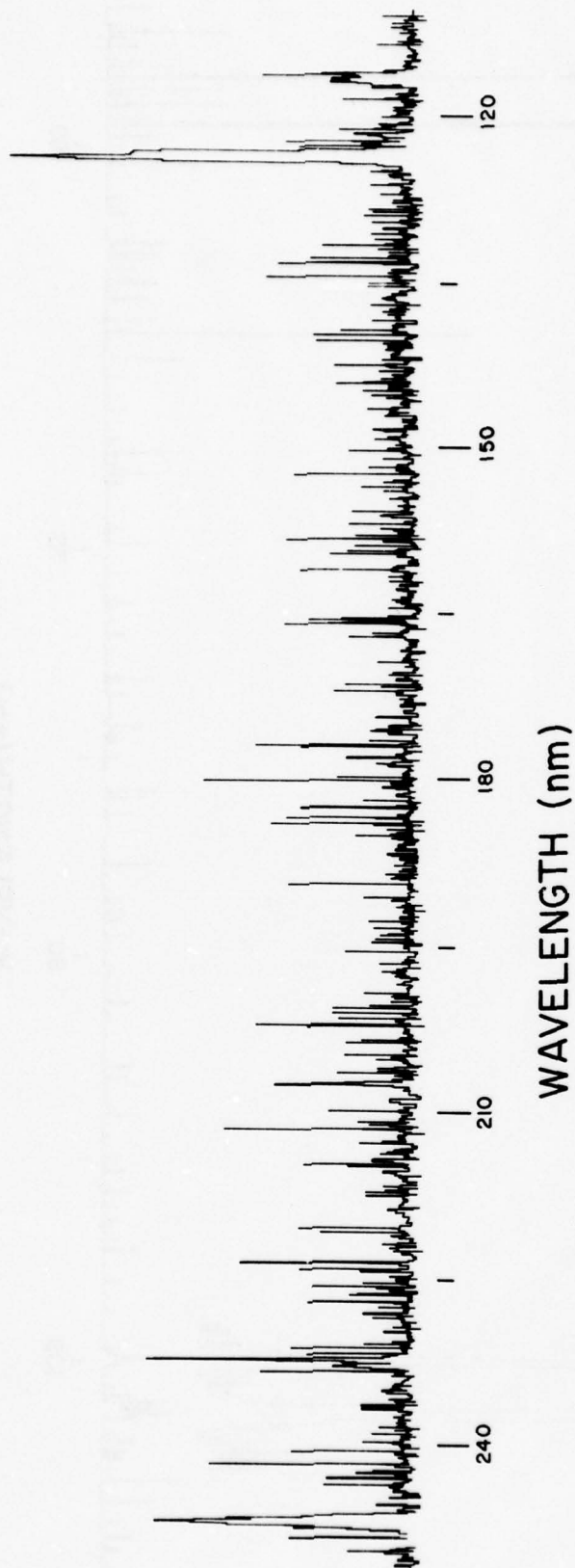
Figure 11. Luminescence Spectrum Over the Region 115-250 nm for 100 eV Impact of Ar_2^+ on Krypton. Ion current 1.1 nA, krypton pressure 2.4 mtorr, counting time 10 s, continuous mode.

34

TABLE 10

Ar_2^+/Kr OBSERVED EMISSIONS

Spectral Range: 55-250 nm
Kinetic Energy: 100 eV

Wavelength (nm)	Grating/ Detector	Classification		Spectrum	Reference	Line Intensity $(cs^{-1} nA^{-1} mtorr^{-1})$	Cross Section $(10^{-16} cm^2)$
		Lower State	Upper State				
104.7 ±0.3	3/1	$3p^6\ ^1S_0$	$4s'[1/2]_1^o$	ArI	a	0.3	0.06
106.6 ±0.3	3/1	$3p^6\ ^1S_0$	$4s[3/2]_1^o$	ArI	a	0.4	0.07
116.2 ±0.3	1/2	$4p^6\ ^1S_0$	$5s'[1/2]_1^o$	KrI	a	< 0.1	< 0.01
123.3 ±0.3	1/2	$4p^6\ ^1S_0$	$5s[3/2]_1^o$	KrI	a	2.0	0.2

[a] See Ref. 32.

35

Figure 12.   Kinetic Energy Dependence of Emission Cross Section for 123.3 nm KrI,
106.6 and 104.7 nm ArI lines in Ar$_2^+$/Kr Collisions.

36

3. Ar_2^+/Ar

In order to complete the series of cross section measurements the reaction (16) was studied by measuring the cross section for the two ArI resonance lines under 100 eV collision conditions.

$$Ar_2^+ + Ar \rightarrow (Ar_2^+) + Ar^*$$ (16)
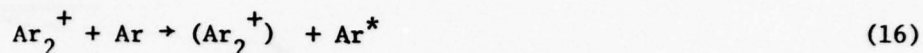
The cross section for exciting Ar 4s $[3/2]_1^o$ and 4s' $[1/2]_1^o$ is less than 0.01×10^{-16} cm^2.

D. Miscellaneous Ion-Atom Reactions

1. Xe^+/Xe

During the course of this study an indepth analysis of the Xe^+/Xe system was completed. The major results of this study are presented in Appendix A in the form of a preprint for subsequent publication.

2. Ar^+/Xe, Kr, Ar

No attempt was made to completely scan all of the emissions for the Ar^+/Xe system under 100 eV collisions; however, the spectral region in the vicinity of the ArI and XeI lowest energy resonance lines was investigated. Over the spectral region 110-200 nm the only emissions observed are shown in Figure 13. These lines are summarized in Table 11. In each case the reactant Ar^+ ions were formed by 31 V electron impact and no further attempt was made to eliminate metastable ions in the ion beam. It is presumed that the beam is comprised principally of Ar^+ $^2P_{3/2,1/2}^o$ approximately in the ratio 2:1.

The reaction of Ar^+ with xenon yields principally ArI and XeI lines analogous to the reactions with the Ar_2^+ colliding ion. The 146.9 nm XeI line arises from reaction (17)[35]

$$Ar^+ + Xe \rightarrow Ar^+ + Xe^* \text{ 6s } [3/2]_1^o - 8.4 \text{ eV}$$ (17)
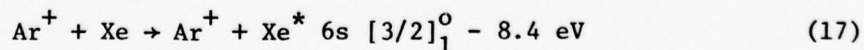
and the 104.7 nm ArI line arises from reaction (18)

$$Ar^+ + Xe \rightarrow Ar^* \text{ 4s' } [1/2]_1^o + Xe^+(^2P_{3/2}^o) - 8.1 \text{ eV}$$ (18)

37
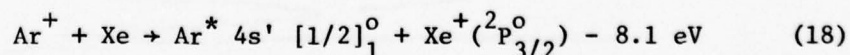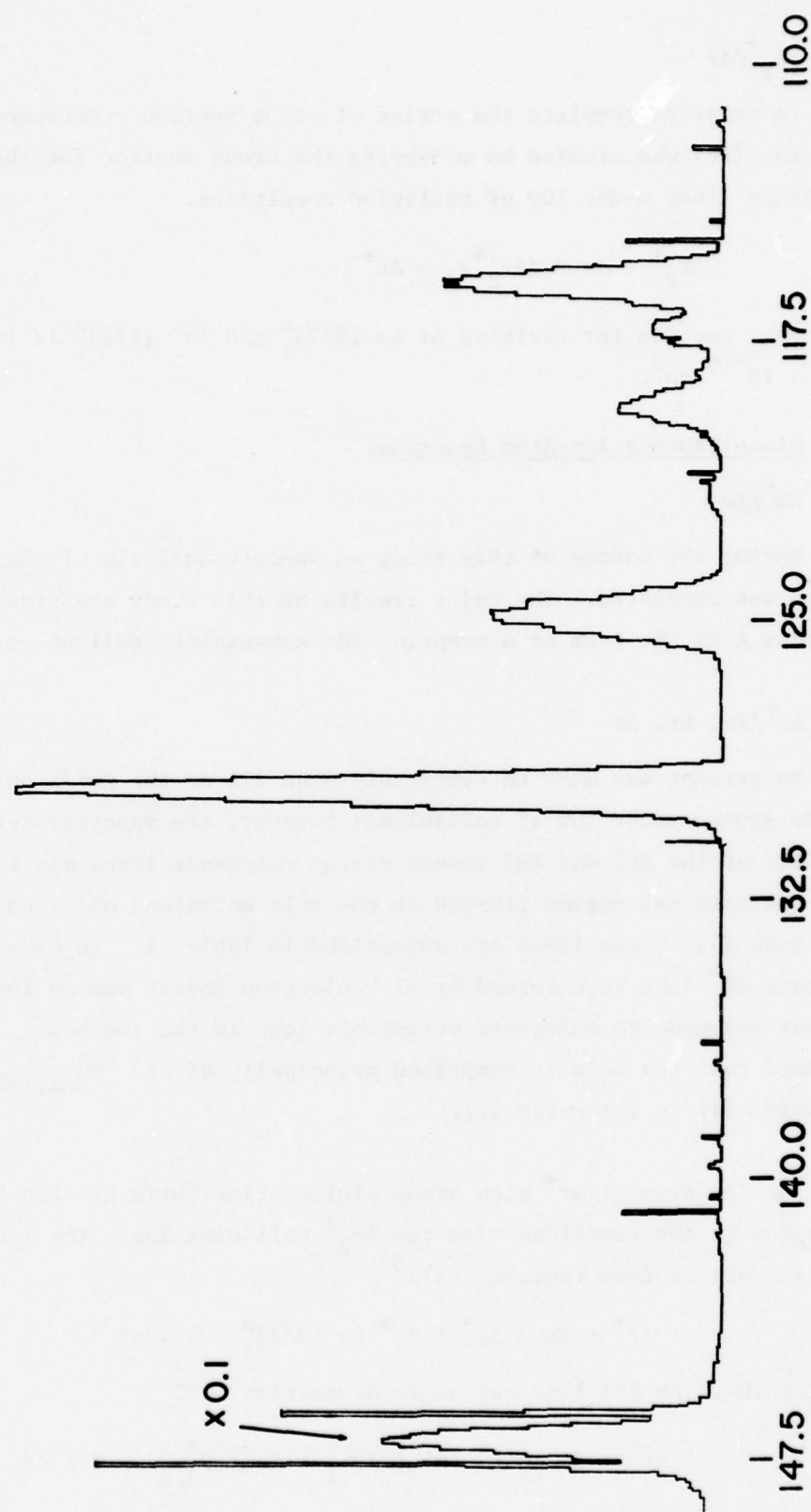
Figure 13. Luminescence Spectrum Over the Range 110-150 nm for 100 eV Impact of Ar$^+$ on Xenon. Ion current 21 nA, xenon pressure 3 mtorr, counting time 10 s, continuous mode.

TABLE 11

Ar$^+$/Xe OBSERVED EMISSIONS

Spectral Ranges 104-107 nm and 110-200 nm

Kinetic Energy: 100 eV, 31 V electron impact for Ar$^+$ formation

Wavelength (nm)	Grating/ Detector	Classification Lower State	Upper State	Spectrum	Reference	Line Intensity (cs^{-1} nA^{-1} mtorr^{-1})	Cross Section (10^{-16} cm^2)
104.7 $\pm$0.3	3/1	$3p^6$ $^1S_0$	$4s'[1/2]^o_1$	ArI	a		~ 0.30
106.6 $\pm$0.3	3/1	$3p^6$ $^1S_0$	$4s[3/2]^o_1$	ArI	a		~ 0.14
115.9 $\pm$0.3	1/2	$5p^5$ $^2P^o_{1/2}$	$5d$ $^4D_{1/2}$	XeII	b		0.08
117.2 $\pm$0.3	1/2	--	--	?			
119.3 $\pm$0.3	1/2	$5p^6$ $^1S_0$	$5d[3/2]^o_1$	XeI	a		< 0.03
124.9 $\pm$0.3	1/2	$5p^6$ $^1S_0$	$5d[1/2]^o_1$	XeI	a		0.06
	1/2	$5p^5$ $^2P^o_{1/2}$	$5p$ ^{6} $^2S_{1/2}$	XeII	b		
129.6 $\pm$0.3	1/2	$5p^6$ $^1S_0$	$6s'[1/2]^o_1$	XeI	a		0.19
146.9 $\pm$0.3	1/2	$5p^6$ $^1S_0$	$6s[3/2]^o_1$	XeI	a		1.1

^{a}See Ref. 32.

^{b}See Ref. 6.

In each case the reaction cross sections for reaction of the argon atomic ion Ar^+ exceed those for the molecular ion, Ar_2^+. This can be correlated approximately with the difference in reaction endothermicity. The kinetic energy dependence of the 146.9 nm XeI line is shown in Figure 14. As with all other reactions observed in this study, endothermic behavior is indicated and a fairly sharp kinetic energy onset is apparent.

Figures 15 and 16 show the energy variation of the KrI and ArI lines from the Ar^+/Kr and Ar^+/Ar reactions, respectively. Because of the presence of some metastable Ar^+ ions in the reactant beam there is some ambiguity concerning the precise reaction onset; however, these onsets have been estimated and are discussed in the following section.

E.   Summary

Table 12 summarizes all of the data obtained for the atomic resonance lines produced in Ar^+ and Ar_2^+ collisions with xenon, krypton and argon. Note the following empirical points from Tables 8 and 12.

- for both collisional excitation and charge-transfer reactions Ar^+ ions are more efficient than Ar_2^+ ions.

- in collisional excitation the emission cross section for the lowest resonance line is always the largest.

- whereas He^+ and He_2^+ tend to react only by charge-transfer, Ar^+ and Ar_2^+ react mainly via collisional excitation. The charge-transfer reaction path producing ArI excitation is available in each case but with lower overall cross section.

- the cross section for collisional excitation by Ar^+ or Ar_2^+ reaction decreases in the series xenon, krypton, argon.

- generally when the two resonance levels $s\ [3/2]_1^0$ and $s'\ [1/2]_1^0$ are populated, the former displays the larger emission cross section with two exceptions. In reactions Ar^+/Xe and Ar_2^+/Xe the emission cross section for Ar $4s'\ [1/2]_1^0$ exceeds that for Ar $4s\ [3/2]_1^0$.

- kinetic energy thresholds for Ar_2^+ reactions always greatly exceed the reaction enthalpy. This indicates very high reaction barriers suggesting that the accompanying products are not formed in the ground electronic state.

40
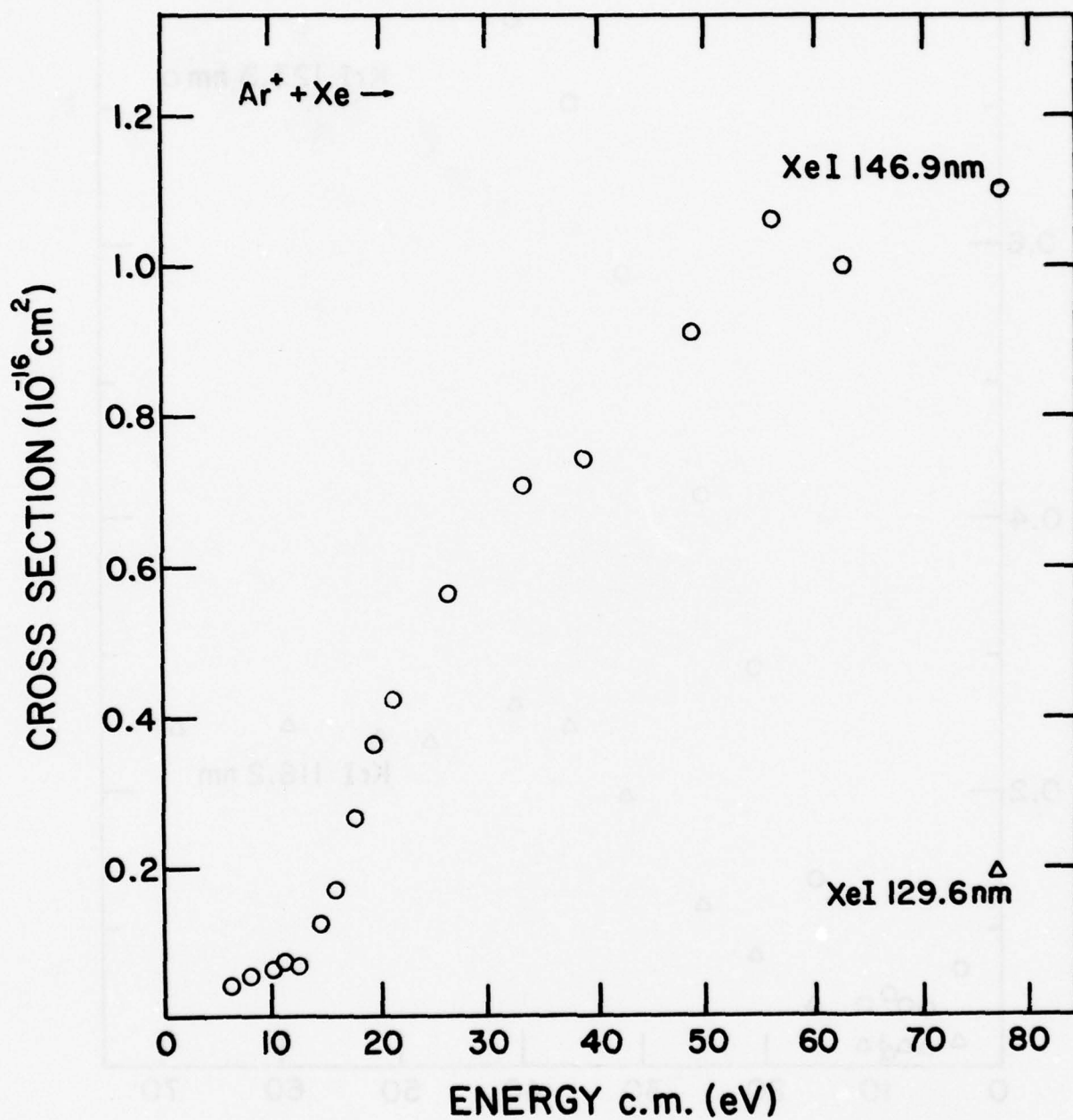
Figure 14.   Kinetic Energy Dependence of Emission Cross Section for 146.9 nm XeI line in Ar+/Xe Collisions

41
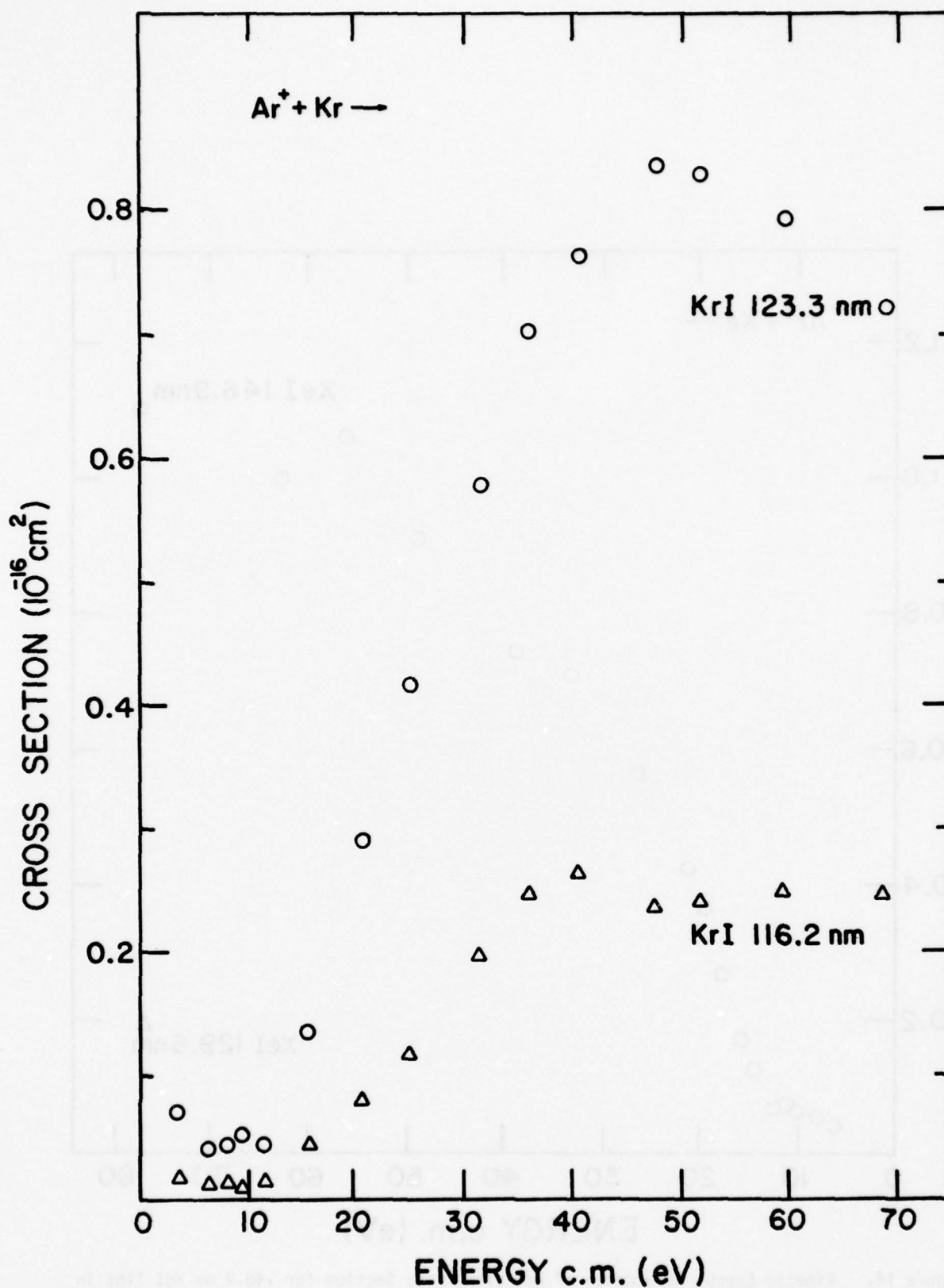
Figure 15. Kinetic Energy Dependence of Emission Cross Section for 123.3 nm and 116.2 nm KrI lines in Ar$^+$/Kr Collisions.

42
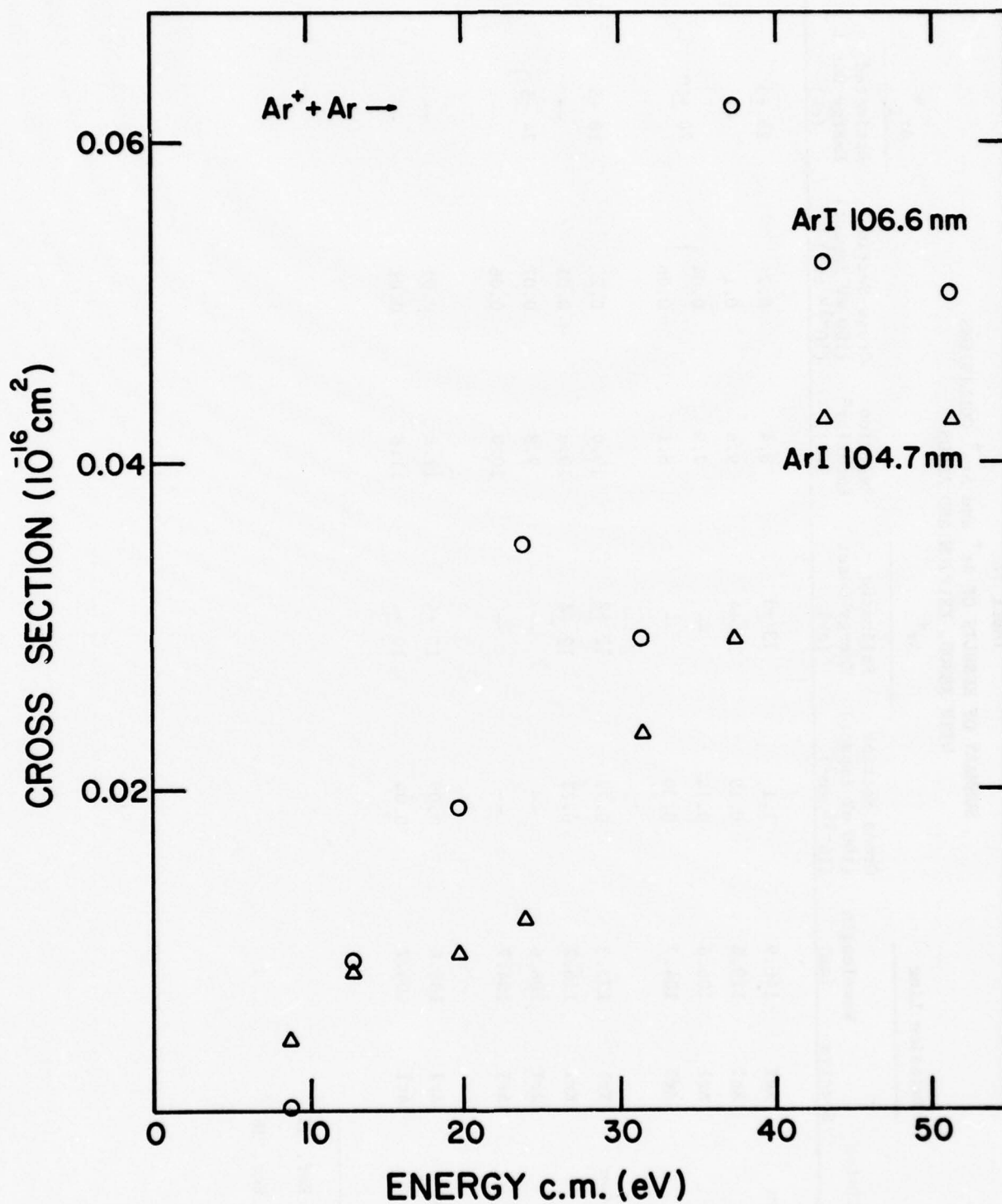
Figure 16.   Kinetic Energy Dependence of Emission Cross Section for 106.6 nm and
104.7 nm ArI Lines in Ar$^+$/Ar Collisions.

43

TABLE 12

SUMMARY OF RESULTS OF Ar^+ and Ar_2^+ COLLISIONS
WITH XENON, KRYPTON AND ARGON

Collision Gas	Emission Line Spectra	Wavelength (nm)	Ar^+ Cross Section (100 eV impact) (10^{-16} cm²)	Ar^+ Estimated Energy Onset (eV)	Ar^+ Reaction Enthalpy[a] (eV)	Ar_2^+ Cross Section (100 eV impact) (10^{-16} cm²)	Ar_2^+ Estimated Energy Onset (eV)	Ar_2^+ Reaction Enthalpy[a] (eV)
Xenon	XeI	146.9	1.1	13 ±3	8.4	0.7	25 ±3	8.4
	XeI	129.6	0.19	12 ±4	9.6	0.1	--	9.6
	ArI	106.6	0.14	--	7.9	0.04 }	20 ±10	> 9.3
	ArI	104.7	0.30	--	8.1	0.06	--	
Krypton	KrI	123.3	0.72	12 ±2	10.0	0.2	18 ±5	10.0
	KrI	116.2	0.22	12 ±4	10.6	< 0.01	--	10.6
	ArI	106.6	--	--	9.8	0.07	24 ±5 }	>11.2
	ArI	104.7	--	--	10.0	0.06	--	
Argon	ArI	106.6	0.05	10 ±4	11.6	< 0.01	--	11.6[b]
	ArI	104.7	0.04	10 ±4	11.8	< 0.01	--	11.8[b]

[a]See Ref. 35.

[b]See Ref. 36.

- all reactions analyzed in this study require the transfer of translational into internal energy; however, the cross sections for reaction in many of the systems are appreciable, indicating efficient energy transfer.

- kinetic energy thresholds for Ar^+ reactions agree within a few volts of the reaction enthalpy.

In ion-atom collisions that yield excited products (excluding particle transfer), there is a competition between the projectile and target for absorbing the excitation. All reactions investigated in this study are endothermic; hence, *transfer of collisional energy into internal energy of the projectile or target occurs.*

Excitation of the projectile He^+ or Ar^+ is manifested by HeII or ArII emissions if the mechanism is collisional excitation. These emissions are not observed in He^+ or Ar^+ collisions, nor are they observed in He_2^+ or Ar_2^+ collisions. Excitation of the projectile can occur during the removal of an electron from the target (i.e., during charge-transfer). Although excitation of the projectile is not observed in He^+ or He_2^+ collisions (i.e., no HeI lines observed) it is quite prevalent in reactions of Ar^+ and Ar_2^+ (i.e., ArI lines observed).

Excitation of the target rare-gas designated Rg, can be classified as collisional excitation if RgI emissions are observed or as charge-transfer excitation if RgII emissions predominate. In all cases target excitation predominates over projectile excitation. With He^+ and He_2^+ impacting ions this is manifested as charge-transfer and with Ar^+ and Ar_2^+ ions this is manifested primarily as collisional excitation.

Since all reactions studied are endothermic, the charge-transfer route is energetically more favorable for impacting ions such as He^+ and He_2^+ having large recombination energies. The smaller the energy defect in the reaction (barring accidental resonance), the smaller the tendency to have the charge-transfer path dominate and the greater the tendency for collisional excitation of the target. Compare, for example, the cross section for producing $S[3/2]_1^o$ is 1.1, 0.72 and 0.5×10^{-16} cm^2

45

for 100 eV Ar^+ collisions with xenon, krypton and argon having ionization potentials 8.4, 10.1 and 11.6 eV, respectively.

The nature of the excitation path appears to be governed by the potential curves or surfaces for the ion-atom systems. As the reactants approach, they can be described as following along one of the available curves. When they approach closely the system rises up the steeper region of the potential curve by means of transferring collisional energy into potential energy of the system. Exit channels are available by means of the system crossing from the incoming curve to an outgoing curve leading to asymptotes associated with excited states of the reactant species. Exit channels leading to the lower-lying states are observed to be the most favorable because the region for the appropriate curve-crossing can occur with the least expenditure of collisional energy.

IV. CONCLUSIONS

Optical excitation in a series of ion-atom reactions has been observed and analyzed. The systems studied include the following molecular ion reactions: He_2^+/Xe, He_2^+/Kr, He_2^+/H_2, Ar_2^+/Xe, Ar_2^+/Kr and Ar_2^+/Ar. The following atomic ion reactions were also studied: Ar^+/Xe, Ar^+/Kr, Ar^+/Ar and Xe^+/Xe. Although considerable work is required in the future to complete the entire study of the rare-gas systems, a consistent view is emerging from the results completed in this investigation. The measurement of state-to-state cross sections for charge-transfer and collisional excitation in endothermic ion-atom reactions has provided better insight into prediction of excitation paths and their relative efficiencies, transfer of translational into internal energy, direct measurements of reaction activation barriers with immediate application to the preparation of potential energy curves for the atomic systems and energy surfaces for the molecular systems and finally the competition between charge-transfer and collisional excitation. The magnitude of the collisional excitation processes, in particular in the Xe^+/Xe system, and the strong dependence on quantum state of the reacting ion indicate that such reactions may play a significant role in determining energy dispersal in energized rare-gas mixtures.

REFERENCES

1. J. L. Franklin, Ed., Ion-Molecule Reactions, Vol. I and II, Plenum Press, New York, 1972.

2. Ion-Molecule Reactions in the Gas Phase, Advances in Chemistry Series, 58, American Chemical Society, Washington, D.C., 1966.

3. P. Ausloos, Ed., Fundamental Processes in Radiation Chemistry, Wiley Interscience, New York, 1968.

4. D. K. Bohme and J. Laudenslager in private communication to the author have reported that the charge-transfer reaction occurs with a rate at or below their detectable limit.

5. E. G. Jones, B. M. Hughes, D. C. Fee and T. O. Tiernan, Phys. Rev. 15, 1446 (1977).

6. a. E. G. Jones, B. M. Hughes, T. O. Tiernan, D. C. Fee and D. G. Hopper, Spectrochimica Acta: in press.

   b. E. G. Jones, B. M. Hughes, T. O. Tiernan, D. C. Fee and D. G. Hopper, Brehm Laboratory Technical Report 10, July 1977, Wright State University.

7. E. G. Jones, T. O. Tiernan, D. C. Fee and B. M. Hughes: submitted to J. Chem. Phys.

8. C. B. Collins and A. J. Cunningham, Applied Physics Letters, 27, 127 (1975).

9. C. B. Collins, A. J. Cunningham and M. Stockton, Applied Physics Letters, 25, 344 (1974).

10. R. D. Reid, J. R. McNeil and G. J. Collins, Applied Physics Letters, 29, 666 (1976).

11. J. R. McNeil, W. L. Johnson, G. J. Collins and K. B. Persson, Applied Physics Letters, 29, 172 (1976).

12. T. Shay, H. Kano and G. J. Collins, Applied Physics Letters, 26, 531 (1975).

13. H. Kano, T. Shay and G. J. Collins, Applied Physics Letters, 27, 610 (1975).

14. W. L. Johnson, J. R. McNeil and G. J. Collins and K. B. Persson, Applied Physics Letters, 29, 101 (1976).

15. R. C. Jensen, G. J. Collins and W. R. Bennett, Jr., Physical Review Letters, 23, 363 (1969).

16. W. K. Schuebel, Applied Physics Letters, 16, 470 (1970).

17. W. T. Silfvast and M. B. Klein, Applied Physics Letters, 17, 400 (1970); 18, 482 (1971).

18. C. B. Collins, A. J. Cunningham, S. M. Curry, B. W. Johnson and M. Stockton, Applied Physics Letters, 24, 477 (1974).

19. J. J. Leventhal, J. D. Earl and H. H. Harris, Physical Review Letters, 35, 719 (1975).

20. D. E. Rothe and K. O. Tan, Applied Physics Letters, 30, 152 (1977).

21. R. A. Waller, C. B. Collins and A. J. Cunningham, Applied Physics Letters, 27, 323 (1975).

22. G. H. Bearman, J. D. Earl, R. J. Pieper, H. H. Harris and J. J. Leventhal, Phys. Rev. A 13, 1734 (1976).

23. G. H. Bearman, H. H. Harris and J. J. Leventhal, Applied Phys. Letters 28, 345 (1976).

24. B. M. Hughes, E. G. Jones and T. O. Tiernan, Abstracts of VIII International Conference on the Physics of Electronic and Atomic Collisions, Vol. I, Institute of Physics, Belgrade, Yugoslavia (1973), p. 223.

25. B. M. Hughes et al.: Instrument paper to be submitted to Rev. Sci. Inst.

26. E. G. Jones, B. M. Hughes, R.L.C. Wu, T. O. Tiernan and D. G. Hopper: submitted to J. Chem. Phys.

27. G. H. Dunn, R. Ceballe and D. Pretzer, Phys. Rev. 158, 29 (1976).

28. J. A. Hornbeck and J. P. Molnar, Phys. Rev. 84, 621 (1951).

29. C. E. Moore, Atomic Energy Levels, NBS Circ. 467, Vols. 1 (1949), 2 (1952), 3 (1958).

30. W. R. Wadt, J. Chem. Phys. 68, 402 (1978).

31. M. S. B. Munson, J. L. Franklin and F. H. Field, J. Phys. Chem. 67, 1542 (1963).

32. A. R. Striganov and N. S. Sventitskii, Tables of Spectral Lines of Neutral and Ionized Atoms (Plenum, New York, 1968).

33. E. G. Jones, T. O. Tiernan, B. M. Hughes and D. C. Fee: to be published.

34. The ground state of xenon has the configuration $5p^6$ and is designated $^1S_0$ in LS notation. The two excited states of xenon populated here have configurations $5p^5(^2P^o_{3/2})6s$ and $5p^5(^2P^o_{1/2})6s$ designated $6s\ [3/2]^o_1$ and $6s'\ [1/2]^o_1$, respectively using Jℓ-coupling notation in the general form.

35. The endothermicity given for these reactions is calculated assuming both reactants and all non-radiating products are in the ground state. In reaction (17), for example it is assumed that Ar^+ is $5p^5\ ^2P^o_{3/2}$.

36. Enthalpy value is calculated assuming that the ArI excitation line arises from collisional excitation as opposed to collisional dissociation of the argon molecular ion.

MANUSCRIPT OF Xe$^+$/Xe STUDY

51

EXCITATION OF Xe I RESONANCE LINES IN Xe^+/Xe COLLISIONS[*]

E. GRANT JONES
Department of Chemistry and The Brehm Laboratory
Wright State University, Dayton, OH 45435

ABSTRACT

Symmetric ion-atom reactions in xenon of the type $Xe^+ + Xe \rightarrow Xe^+ + Xe^*$ have been found to occur with large cross sections at collision energies below 50 eV (c.m.). The reaction cross section for production of the two lowest Xe resonance levels $6s[3/2]_1^o$ and $6s'[1/2]_1^o$ at collision energies from 7-50 eV have been measured by monitoring the 147.0 nm and 129.6 nm Xe I lines. All reactions involving $Xe^+(^2P_{3/2,1/2}^o)$ impacting ions display kinetic energy thresholds corresponding to the transfer of more than 11 eV of translational energy into internal energy. Experimental kinetic energy thresholds exceed the energy difference between the reactants and products taken at infinite separation. Excitation of the lowest resonance level of Xe $6s[3/2]_1^o$, is found to depend strongly on the electronic state, $^2P_{3/2}^o$ or $^2P_{1/2}^o$, of the reacting xenon ions.

52

INTRODUCTION

Several groups[1-7] have measured cross sections under low collision energy (1-100 eV) conditions for the symmetric resonant charge-transfer reaction (1) in xenon. Such reactions are thought to occur by means of a long-range electron jump in which there is very little momentum transfer.

$$Xe^+(^2P_J^o) + Xe(^1S_o) \overset{\sigma_1}{\to} Xe(^1S_o) + Xe^+(^2P_J^o) \tag{1}$$
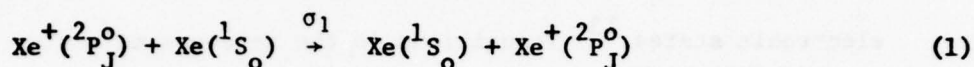
Theoretical two-state one-electron treatments[8,9] are generally consistent with the experimentally measured kinetic energy behaviour and cross section $(40\text{-}100 \times 10^{-16} cm^2)$.

Reactions of Xe^+ with xenon have been analyzed in the present study as part of an investigation into the anomalous presence of Xe I resonance lines in the emission spectrum produced during He^+/Xe collisions.[10,11] One of the possible explanations, based on an earlier study in this laboratory, was that Xe I resonance lines arose not from He^+/Xe collisions but rather from secondary reactions of the Xe^+ ionic products with xenon. To verify these ideas, light emitted by short-lived species ($\tau < 10^{-6}$s) produced in collisions of Xe^+ ions with xenon was analyzed.

The two major reactions that produce radiating products are depicted by

$$Xe^+(^2P_J^o) + Xe(^1S_o) \overset{\sigma_2}{\to} Xe^+ + Xe\ 6s[3/2]_1^o \tag{2}$$

$$Xe^+(^2P_J^o) + Xe(^1S_o) \overset{\sigma_3}{\to} Xe^+ + Xe\ 6s'[1/2]_1^o \tag{3}$$
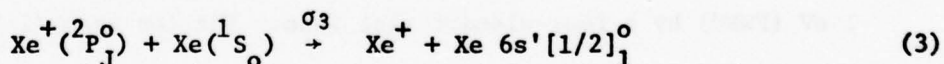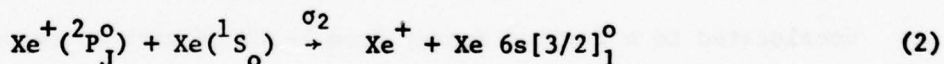
the reactions (2) and (3). The ground state of Xe has the configuration $5p^6$ and is designated ^1S_o in LS notation. The excited states of Xe produced in these reactions have configurations $5p^5(^2P_{3/2}^o)6s$ and $5p^5(^2P_{1/2}^o)6s$ designated $6s[3/2]_1^o$ and $6s'[1/2]_1^o$, respectively, using Jl-coupling notation

53

in the general form.[12] These reactions are symmetric, but not resonant, and involve strong collisions, during which a significant fraction of translational energy of approach (T) is converted into internal energy (I) of the system. Reactions of this type, involving translational-to-internal (T→I) energy conversion provide important information concerning the potential curves of the rare-gas molecular ions and their excited molecular electronic states.[13] Transitions in the rare-gas molecular ions are potential candidates for laser action in the visible, ultraviolet and vacuum ultraviolet spectral regions.

In this report, the cross sections σ_2 and σ_3, and kinetic energy dependence of reactions (2) and (3) are presented and compared to reaction (1). Reactions (2) and (3) are discussed as regards the total angular momentum quantum number J of the reactant ions.

EXPERIMENTAL

A. Apparatus

The optical emissions apparatus (OEA) used in this study has been described elsewhere.[14,15] Briefly, it consists of a single-focussing mass spectrometer in which Xe^+ ions are formed by electron impact and accelerated to 1.1 kV. The $^{132}Xe^+$ isotopes are mass-selected and decelerated to a desired energy from 1-100 eV with an energy spread of 1 eV (FWHM) by a four-element slot lens. The ion beam (1-20 nA) is chopped at 1 kHz by a 100 V deflection pulse, then allowed to pass through a differentially-pumped collision chamber of path length 0.475 cm containing xenon gas[16] at a pressure from 1-2 mtorr. Attenuation of the ion beam due to reaction and scattering in the collision chamber is less than 20%. Excited products formed in this region can subsequently radiate in

54

the absence of significant perturbations from electric fields (< 0.1 V cm^{-1}),
magnetic fields (< 1G) and collisions.[17] No effects of resonance absorption
of emitted light have been detected for collision chamber pressures up to
4 mtorr.

Light produced by short-lived species formed in the collision chamber
is monitored in the direction of the ion beam with a McPherson 1-m VUV
monochromator. In this region background pressure is typically 4 x 10^{-6}
torr. A combination of a Bausch and Lomb grating,[18] blazed at 200 nm,
and EMR photomultiplier tube[19] are used in conjunction with an SSR Model 1110
photon counter to measure the radiation in the 115-290 nm interval. Scans
from 300-600 nm were taken using a Bausch and Lomb grating,[20] blazed at
500 nm and RCA-C31034A photomultiplier tube to investigate possible
cascading into the Xe I resonance levels $6s[3/2]_1^o$ and $6s'[1/2]_1^o$. Under
100 eV (lab) collision conditions, no radiation from other states cascading
into these levels was detected, leading to an estimate of 10^{-18} cm^2 as
an upper limit to the cross section for cascading contributions. Additional
investigations over the interval 60-110 nm using a Channeltron detector
revealed no optical emissions with cross section exceeding 2 x 10^{-18} cm^2.

B.   Experiments

The collision energy for reactions (2) and (3) was varied from 10-100 eV
(lab) and the intensity of the two major[21] Xe I lines at 147.0 nm,
(^1S_o) ← $6s[3/2]_1^o$, and 129.6 nm, (^1S_o) ← $6s'[1/2]_1^o$, was monitored at a
spectral resolution of 1.5 nm (FWHM), counting photon pulses for periods
up to two minutes. Phase sensitive detection eliminates problems arising
from stray light originating in the ion-source region or light emanating
from possible collisions occurring within the deceleration lens.

Because of strong spin-orbit interactions in Xe $(^2P^o_{3/2}$--$^2P^o_{1/2}$ splitting is 1.31 eV), it is possible, using electron impact, to prepare $^{132}Xe^+$ ions below the appearance potential for the J = 1/2 state. Thus, by increasing the ionizing voltage, the composition of the reactant ion beam can be varied from 100% J = 3/2 down to percentages close to the statistical limit of 67% at high ionizing voltages. To investigate the effects of J on the course of reactions (2) and (3), kinetic energy experiments were performed employing the lowest ionizing voltage that afforded a usable ion beam. Under these conditions, it was assumed that the reactant beam was comprised entirely of Xe^+ $(^2P^o_{3/2})$. Most of the other experiments were completed using 30 V ionizing electrons. Under these ionizing conditions Amme and Haugsjaa[6] have concluded from the selective charge-transfer reaction between Xe^+ and oxygen that the beam consists of 77 $\pm$3% $^2P^o_{3/2}$. In the present study it is assumed that under 30 V ionizing conditions 77% of the beam is $^2P^o_{3/2}$. Metastable ions, having appearance potentials in excess of 11.8 eV, are considered to make only a small contribution. Short-lived excited ions radiate during the 10-20 μs required to reach the collision region and make a negligible contribution to the reacting beam.

C. Calibration

Cross sections for Xe I transitions are measured relative to the cross section for a reference reaction; namely, Lyman-alpha production (121.6 nm) in 100 eV collisions of He^+ ions with hydrogen. Using the OEA apparatus, under similar conditions to the present study, a cross section of 0.60×10^{-16} cm^2 has been reported,[22] in good agreement with the value of Dunn et al.[23] No attempt has been made to correct for variations in the spectral response of the system over the range 121.6-147.0 nm. The quantum

56

efficiency of the detector is flat in this interval; however, expected variations in grating reflectance would cause an overestimation of the 147.0 nm line intensity. The effect, less pronounced for the 129.6 nm line, is considered to be smaller than a factor of two for both line intensities.[24] Implicit in cross section determinations from experiments of this type is that all radiation is emitted isotropically and without polarization. Overall, cross sections directly measured in the present study are conservatively estimated to be accurate within a factor of five, and the relative comparisons of the XeI lines within a factor of two.

RESULTS AND DISCUSSION

A. Kinetic Energy Behaviour of Reactions (2) and (3)

Since cascading effects were found to be negligible, the cross sections σ_2 and σ_3 for reactions (2) and (3) are given by the total emission cross section for the 147.0 nm and 129.6 nm lines, respectively. These are shown in Fig. 1, for reaction of $^{132}Xe^+$ ions prepared under 30 V ionizing conditions, over the kinetic energy region from 7-50 eV (c.m.). Cross sections are calculated assuming the $^2P^o_{3/2,1/2}$ states of the xenon ion react with equal efficiency. Both reactions display endothermic behaviour, having kinetic energy thresholds, above which the cross section increases approximately linearly with energy. The lowest energy resonance level, $6s[3/2]^o_1$, is populated about ten times more efficiently than the next resonance level, $6s'[1/2]^o_1$. Cross sections for both reactions are large, considering the requirement that more than 11 eV of translational energy must be converted into internal energy. The apparent thresholds for (2) and (3) are 11.5 $\pm$0.5 eV and 12 $\pm$2 eV, respectively.

57

Two other items are apparent in Fig. 1. The scatter in the data, particularly at the higher collision energies, is caused in part by the presence of two sets of independent data points. More recent studies in this region indicate that there is no marked oscillatory structure like that observed in several other ion-atom systems.[25] At kinetic energies below the apparent threshold, reaction is still observed. In this case, the effect is caused primarily by the presence of a small fraction of excited xenon ions in the reactant beam. Xenon metastable ions such as $5d^4D_{7/2}$, $5d^4F_{9/2,7/2,5/2}$ and $5d'^2F_{7/2}$ possess sufficient excitation energy to undergo exothermic reactions with xenon to populate the observed radiating states, without the need for $T \rightarrow I$ energy conversion. This is discussed further in part D of this section.

B. Role of Ion-source Conditions in Determining the State Distribution of the Xenon Ion Beam

1. Ionizing electron voltage

If all xenon ions present in the beam react similarly, then, altering the ionization voltage, thereby changing the ratio of the distribution of the $^2P^o_{3/2}$ and $^2P^o_{1/2}$ states, should not affect the measured reaction cross section. Reaction (2) was chosen to test this point because of its larger cross section. In Fig. 2, σ_2 under 100 eV (lab) collision conditions, as represented by the emission cross section for the 147.0 nm line, is plotted as a function of the electron ionizing voltage.[26] It should be noted that the cross section calculation takes into account variation of reactant ion beam current with changing ionization conditions. Superimposed on Fig. 2 is the $^{132}Xe^+$ ionization efficiency curve as measured by the reactant ion current at the collision chamber. Despite a wide spread in the electron

58

energy, as evidenced by the low energy tail on the ionization curve, marked effects of xenon ion distribution changes are evident. From the onset of ionization (IP Xe is 12.1 eV), up to 24 V ionizing energy only the ratio of the ground, $^2P^o_{3/2}$, and first excited, $^2P^o_{1/2}$, states of the xenon ion can change. At higher energies metastable ions can be produced in the ion-source and subsequently undergo reaction in the collision chamber.

The conclusions from Fig. 2 are the following. The cross section σ_{2_a}, for reaction (2) with $J = 3/2$, is the limiting value for (2)

$$Xe^+(^2P^o_{3/2}) + Xe(^1S_o) \xrightarrow{\sigma_{2_a}} Xe^+ + Xe\ 6s[3/2]^o_1 \qquad (2_a)$$
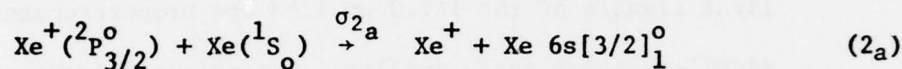
determined under the lowest energy ionization conditions. From Fig. 2, σ_{2_a} can be estimated as $1.4 \times 10^{-16}\ cm^2$. The rapid increase of σ_2 in Fig. 2 arises from the contribution of reaction (2_b)

$$Xe^+(^2P^o_{1/2}) + Xe(^1S_o) \xrightarrow{\sigma_{2_b}} Xe^+ + Xe\ 6s[3/2]^o_1 \qquad (2_b)$$
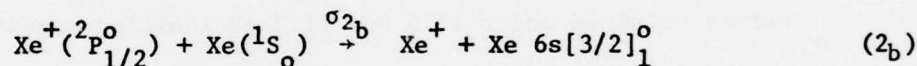
that becomes important as the fraction of reacting xenon ions in the $^2P^o_{1/2}$ level increases. Using σ_2 obtained from Fig. 2 at 30 eV ionizing energy, Amme and Haugsjaa's value[6] for the ion beam abundance ratio and the above estimate for σ_{2_a}, σ_{2_b} can be estimated as $11 \times 10^{-16}\ cm^2$ for 100 eV collisions.

2. Pressure of xenon

In view of the strong dependence of reaction (2) on the total angular momentum quantum number of the reactant xenon ion, the possibility of collisional quenching altering the $^2P^o_{3/2} -- {}^2P^o_{1/2}$ ratio in the ion-source was investigated. Under 30 V ionizing conditions σ_2, measured for 100 eV (lab) collisions, changed less than 3% as a result of pressure changes

59

ranging from a factor of three increase down to a two order of magnitude decrease. No noticeable effects of collisional quenching in the ion-source could be detected.

C. Distribution of Xenon Reactant Ions and the Kinetic Energy Variation of Reaction (2)

Under 11.7 eV ionizing conditions (see Fig. 2), it is assumed that the reactant ion beam is exclusively Xe^+ ($^2P^o_{3/2}$). Since the reactant beam current is reduced by a factor of fifty at this ionizing voltage, detected light signals of the 147.0 nm line are proportionately weaker and the signal-to-noise ratio smaller. The measured cross section, σ_{2_a}, obtained under the same collision conditions employed to obtain Fig. 1, is given by the lower curve in Fig. 3. Because of the reduced signals, more scatter is apparent and the precise reaction onset is more uncertain. Additional curves obtained under 11.6 and 11.8 eV ionizing conditions are not distinguishable from Fig. 3, indicating that contributions of the first excited state, $^2P^o_{1/2}$, can be neglected. Knowing the dependence of σ_{2_a} on kinetic energy, for every data point $(\sigma_2)_{30eV}$ in Fig. 1, σ_{2_b} can be calculated using the relation (4)

$$(\sigma_2)_{30eV} = f_a \, \sigma_{2_a} + f_b \, \sigma_{2_b} \qquad (4)$$

where f_a and f_b are 0.77 and 0.23 respectively based on the data of Amme and Haugsjaa.[6] The upper curve in Fig. 3 shows the computed kinetic energy behaviour of σ_{2_b}. The kinetic energy onset is the same as obtained in Fig. 1. Taking into account the quoted uncertainty[6] of ± 0.03 in f_a and f_b could lead to 30% uncertainty in σ_{2_b}; however, this correction factor is not dependent on collision energy and it will remain constant over the entire range of Fig. 3.

60

As was indicated in section B1, based on data for 100 eV collisions, σ_{2_a} is approximately one-tenth σ_{2_b} at all collision energies from reaction onset to 50 eV.

Using xenon ions formed by 11.7 or 30 V electron impact, no difference between the cross section for reaction (3) could be detected. The pronounced effects of reactant ion-beam composition, so apparent in reaction (2), are not evident for reaction (3). As a result, the lower curve of Fig. 1 is representative of reaction (3) involving xenon ions in either $^2P^o_{3/2}$ or $^2P^o_{1/2}$ states.

D.   Summary

1. Non-zero baseline and effect of exothermic reaction channels

The experimental thresholds and cross sections for 100 eV (lab) collisions are summarized in Table I. Cross sections, in each case, are evaluated from Figs. 1 and 3, taking into account the non-zero baseline below the apparent reaction threshold. To confirm that the principal cause of this correction is the presence of excited xenon metastable ions in the reacting Xe^+ beam, some additional points were taken at lower kinetic energies, under the same collision conditions used for Fig. 1. The apparent cross section, σ_2, is flat from 11 eV down to 3 eV (c.m.) collision energy, then rises sharply at lower energies, indicative of an exothermic reaction. Based on estimates[27,28] of 1% metastable xenon ion abundance under 30 V ionizing conditions, the reaction cross section (at collision energies below 2 eV) exceeds 10^{-14} cm^2. Because of their large reaction cross section, collisions of metastable xenon ions[29] with xenon may account for the anomalous Xe I lines in the He^+/Xe collision spectrum. The difficulty in He^+/Xe collisions, of producing xenon ions

61

possessing sufficient kinetic energy to overcome the barrier to reaction (2) or (3), precludes consideration of the contribution from reaction of Xe ($^2P^o_{3/2,1/2}$).

2. Reaction (2)

The kinetic energy thresholds for reaction (2) are listed in Table I. Reaction involves the transfer of at least 10 eV of translational into potential energy to overcome the reaction barrier. Unlike the resonant charge-transfer reaction (1), the close collisions required for the extensive energy conversion result in significant momentum in both reaction products. Reaction symmetry precludes, in the present study, classification of reaction (2) as charge-transfer or collisional excitation; however, the absence of Xe II lines in the luminescence spectrum strongly suggests the latter. Determination of the isotopic distribution of the product xenon ions could verify this. There is a similar ambiguity as to the state ($^2P^o_{3/2}$ or $^2P^o_{1/2}$) of the product xenon ions. The experimentally determined threshold of 11.5 $\pm$0.5 eV for reaction (2_b) exceeds the calculated energy difference between the reactants and products taken at infinite separation by 4.4 $\pm$0.5 eV or 3.1 $\pm$0.5 eV depending on the state of the product xenon ion.

As $Xe^+(^2P^o_{1/2})$ and $Xe(^1S_o)$ approach, two strongly repulsive potential curves $^2\Pi_{1/2u}$ or $^2\Sigma^+_g$ can describe the resultant molecular system.[13,30] Reaction (2_b) may be described schematically in Fig. 4 in which the relative energies of the reactant and product channels are depicted along with the calculated potential curves of Wadt.[31] The dashed line is an extrapolation of the potential curves for the incoming channels to higher potential energies. The kinetic energy of the ion and atom approaching along channel B of Fig. 4 is converted into potential energy as the particles near the

62

strongly repulsive region. In the vicinity of 11-12 eV above the asymptotic limit, there is a region where the potential curves for the incoming and exiting systems "cross" leading to $Xe^+ + Xe \, 6s[3/2]_1^o$. The magnitude of the cross section for this process would indicate that the "curve-crossing" is extremely efficient and specific.[32]

As $Xe^+(^2P_{3/2}^o)$ and $Xe(^1S_o)$ approach along channel A of Fig. 4, four potential curves, $^2\Sigma_u^+$, $^2\Pi_{3/2g}$, $^2\Pi_{1/2g}$ and $^2\Pi_{3/2u}$ can describe the system.[13,30] The $^2\Sigma_u^+$ curve is strongly bound ($D_e = 0.65$[13], 0.79[31] eV), corresponding to the stable Xe_2^+ molecular ion. The present experiments do not probe the lower energy region of these curves because the kinetic energy restrictions at onset require the system to rise up the steep repulsive region of the incoming channel. Reaction (2_a) involves "curve-crossing" to an exit channel leading to $Xe^+(^2P_{3/2,1/2}^o) + Xe \, 6s[3/2]_1^o$. Excitation of $Xe \, 6s[3/2]_1^o$ is ten times more efficient when the reactants approach along incoming channel B (see Fig. 4) than along channel A. There may be several reasons for this difference. Reactants approaching along channel B have 1.31 eV of internal energy with respect to reactants approaching along channel A so that excitation of $Xe \, 6s[3/2]_1^o$ is less endothermic. Although the barrier to reaction (2_b) has been located within limits of ± 0.5 eV, there is considerably more uncertainty in locating the onset for (2_a). Conceivably reaction (2_a) involves multiple curve-crossing further up the steep potential wall and thus may compete with other reaction channels leading to elastic scattering or other products, for example, $Xe \, 6s[1/2]_1^o$. Not all potential curves associated with incoming channels A and B can efficiently cross the potential curves leading to the observed products. If, for example, only one curve from each incoming channel leads to efficient reaction, then incoming channel B would have a statistical edge because of the lesser

63

number of unproductive paths. Crossing of the system between curves associated with the same asymptote leads to elastic collision events.

At the region of crossing in reaction (2_b) the system has 12.8 ± 0.5 eV of energy with respect to the lowest energy asumptote of the Xe_2^+ system. Of the total energy available, $66 \pm 3\%$ or $76 \pm 3\%$ is partitioned into internal energy depending on whether the product ion is Xe^+ $(^2P_{3/2}^o)$ or Xe^+ $(^2P_{1/2}^o)$, respectively. The remainder of the energy is equally divided as kinetic energy of the separated products. Thus $Xe^+(^2P_{1/2}^o)$ or $Xe^+(^2P_{3/2}^o)$ that are the products of reaction (2_b) will separate from xenon under conditions of reaction onset with 1.5 eV or 2.2 eV of energy, respectively, in the center of mass. At higher collision energies the separation energy will increase.

3. Reaction (3)

Production of Xe $6s'[1/2]_1^o$ can be explained qualitatively in the same manner as Xe $6s[3/2]_1^o$ production. The measured cross section and the corresponding thresholds for reactions (3_a), (3_b) and (2_a) are comparable. Each of these reactions is at least as efficient as the most efficient channel leading to excited products in the He^+/Xe and He^+/Ne systems[15,33] in which reaction has been similarly explained in terms of curve-crossing. Reaction (3) occurs with a large cross section, but in this particular system the less endothermic reaction (2_b) dominates, presumably because it involves curve-crossing at a lower region of the repulsive potential curves.

It is of interest at this point to focus attention on the fact that at the region of crossing, the potential curves for the incoming and outgoing channels will be almost parallel because of the appreciable reverse activation

64

energy. Thus, whether reaction occurs via a crossing or an avoided crossing there is no sudden change required in either the position or momentum of the particles during reaction. This is consistent with the observed extensive linear behaviour in Fig. 1 where the cross section increases linearly from onset over a region of about 60 eV energy in the laboratory.

4. Comparison with resonant charge-transfer

Reaction of $Xe^+(^2P^o_{3/2})$ with xenon is dominated by resonant charge-transfer over the entire collision energy regime. On the other hand, for collision energies above 20 eV (lab), reaction (2_b) involving $Xe^+(^2P^o_{1/2})$ can occur in conjunction with resonant charge-transfer. That is, resonant charge-transfer can take place numerous times at long-range as the particles approach; however, at smaller internuclear separations, the momentum transfer inelastic reactions dominate. Helm[34] has measured the mobility of Xe^+ in the $^2P^o_{3/2}$ and $^2P^o_{1/2}$ states in xenon. He concluded for the thermal energy range that there is a kinetic energy *dependent difference* in the charge-transfer cross section of Xe^+ ions in xenon depending on their spin state.[34,35] Thus, the different spin states of Xe^+ display differences both in their charge-transfer and collisional excitation reaction with xenon.

CONCLUSIONS

Behaviour of the cross section, for several excitation reactions arising from Xe^+ + Xe collisions, has been measured as a function of reaction kinetic energy. All reactions leading to Xe I excitation involve large energy barriers that can be surmounted by utilizing the translational energy of approach. Once the energy requirements are met, excitation processes that preferentially populate the lowest radiative levels of Xe I are observed to

65

occur with cross section increasing approximately linearly with kinetic
energy up to 100 eV (lab). No Xe II excitation is observed. It has been
shown that the efficiency of Xe I excitation depends strongly on the state
of the impacting xenon ion. Reaction of the first excited state of the
xenon ion, $(^2P^o_{1/2})$, leading to the lowest energy radiative channel,
$Xe^+ + Xe\ 6s[3/2]^o_1$, occurs with the highest measured cross section. Evidence
that collisions of xenon metastable ions with xenon are highly efficient in
populating $Xe\ 6s[3/2]^o_1$ and $Xe\ 6s'[1/2]^o_1$ via exothermic channels has also
been obtained. The occurrence of such reactions as secondary processes in
early He^+/Xe studies can account for the anomalous Xe I lines present
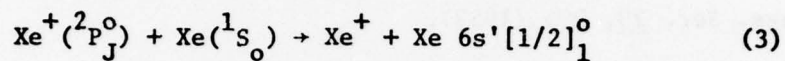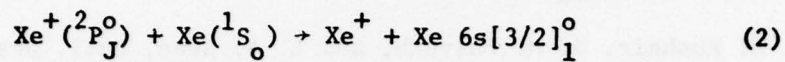in a predominantly Xe II emission spectrum.

Information concerning the potential curves of the Xe^+_2 system has been
obtained. The highly specific nature of the collisional excitation may pro-
vide a new route to achieve states of Xe_2^{+*} that may be potential candidates
for laser action.

ACKNOWLEDGEMENTS

TABLE I

ENERGY THRESHOLD AND REACTION CROSS SECTION SUMMARY

$$Xe^+(^2P_J^o) + Xe(^1S_o) \rightarrow Xe^+ + Xe\ 6s[3/2]_1^o \qquad (2)$$

$$Xe^+(^2P_J^o) + Xe(^1S_o) \rightarrow Xe^+ + Xe\ 6s'[1/2]_1^o \qquad (3)$$

State of Xe^+ Reacting Ion	Kinetic Energy Threshold c.m. (eV)		Cross Section for 100 eV (lab) Collisions ($10^{-16}\ cm^2$)	
	(2)	(3)	(2)	(3)
$^2P_{3/2}^o$	12 ±2	12 ±2	1.1	0.3
$^2P_{1/2}^o$	11.5 ±0.5	12 ±2	11.0	0.3

67

REFERENCES

1. B. Ziegler, Z. Phys. $\underline{136}$, 108 (1953).

2. J. A. Dillon, Jr., W. F. Sheridan, H. D. Edwards and S. N. Ghosh, J. Chem. Phys. $\underline{23}$, 776 (1955).

3. R. M. Kushnir, B. M. Palyukh, and L. A. Sena, Bull. Acad. Sci. U.S.S.R. Phys. Ser. $\underline{23}$, 995 (1959).

4. I. Popescu-Iovitsu, Rev. Roum. Phys. $\underline{4}$, 199 (1959).

5. A. Galli, A. Giardini-Guidoni, and G. G. Volpi, Nuovo Cimento $\underline{26}$, 845 (1962).

6. R. C. Amme and P. O. Haugsjaa, Phys. Rev. $\underline{165}$, 63 (1968).

7. L. Squires and T. Baer, J. Chem. Phys. $\underline{65}$, 4001 (1976).

8. E. F. Gurnee and J. L. Magee, J. Chem. Phys. $\underline{26}$, 1237 (1957).

9. D. Rapp and W. E. Francis, J. Chem. Phys. $\underline{37}$, 2631 (1962).

10. F. J. DeHeer, B. F. J. Luyken, D. Jaecks, L. Wolterbeek Muller, Physica $\underline{41}$, 583 (1969).

11. See discussion by E. W. Thomas in Excitation in Heavy Particle Collisions pp. 203 (Wiley-Interscience, New York, 1972).

12. C. E. Moore, Atomic Energy Levels, Vol III, National Bureau of Standards, Circular 467, U.S. Dept. of Commerce.

13. R. S. Mullikan, J. Chem. Phys. $\underline{52}$, 5170 (1970).

14. B. M. Hughes, E. G. Jones and T. O. Tiernan, Abstracts of VIII International Conference on the Physics of Electronic and Atomic Collisions, Vol I, Institute of Physics, Belgrade, Yugoslavia (1973), p. 223.

15. a. E. G. Jones, B. M. Hughes, D. C. Fee and T. O. Tiernan, Phys. Rev. A $\underline{15}$, 1446 (1977).

    b. E. G. Jones, D. C. Fee, T. O. Tiernan and B. M. Hughes: submitted for publication.

68

16. Xenon, obtained from Matheson as Research Grade, was used without further purification.

17. E. G. Jones, B. M. Hughes, T. O. Tiernan, D. C. Fee and D. G. Hopper, Spectrochim. Act., in press.

18. Bausch and Lomb grating serial no. 2571-5-3, 600 grooves mm^{-1}, MgF_2 coated.

19. EMR Photoelectric serial no. 541F-08-18-03900 photomultiplier tube with MgF_2 window.

20. Bausch and Lomb grating serial no. 2530-6-4-3, 600 grooves mm^{-1}.

21. A third Xe I line observed at 125.0 nm, $(^1S_o) \leftarrow 5d[1/2]_1^o$, with emission cross section $\sim 10^{-17}$ cm^2 was too weak to study with these techniques.

22. E. G. Jones, B. M. Hughes, R. L. C. Wu, T. O. Tiernan and D. G. Hopper: submitted to J. Chem. Phys.

23. G. H. Dunn, R. Geballe and D. Pretzer, Phys. Rev. $\underline{158}$, 29 (1967).

24. Although the grating is blazed at 200 nm, relative intensities of the Lyman-alpha line in the first order (121.6 nm) and second order (243.2 nm) are approximately equal.

25. The He^+/Ne system, for example, displays Landau-Zener-Stuekelberg oscillations that have been well characterized. See B. Andreson, K. Jenson and E. Veje, Phys. Rev. A $\underline{16}$, 150 (1977), and references therein.

26. The ionizing voltage scale has not been calibrated. The onset of the ionization efficiency curve plotted in Fig. 2 is within one volt of the ionization potential for Xe, so that the scale correction is less than one volt.
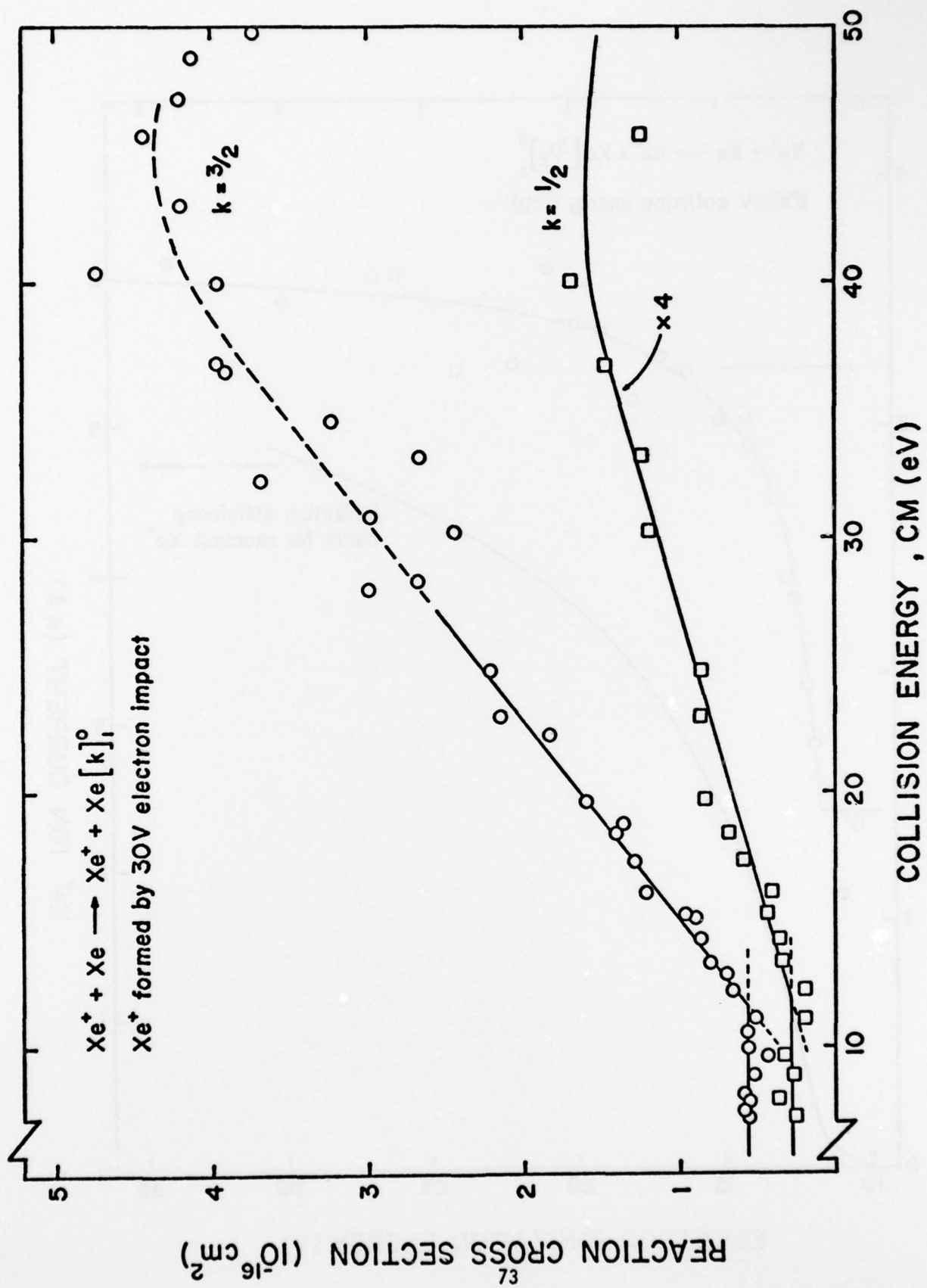
27. P. R. Jones, G. M. Conklin, D. C. Lorents and R. E. Olson, Phys. Rev. A $\underline{10}$, 102 (1974).

28. H. D. Hagstrum, Phys. Rev. $\underline{104}$, 309 (1956).

29. The lowest energy xenon metastable ions are $5d^4D_{7/2}$, $5d^4F_{9/2,7/2,5/2}$ and $5d'^2F_{7/2}$ (see Ref. 15b).

30. H. U. Mittman and H. P. Weise, Z. Naturforsch. $\underline{29\ a}$, 400 (1974).

31. W. R. Wadt, J. Chem. Phys. $\underline{68}$, 402 (1978).

32. The maximum in the total cross section for excited state production from He$^+$/Xe collisions is similar to the total in the present study.[15] However, the energy is distributed over many states of Xe$^+$, and the maximum cross section for producing one particular state of Xe$^+$ is less than 0.3×10^{-16} cm^2. This is contrasted with the high cross section for Xe $6s[3/2]_1^o$ excitation in the Xe$^+$/Xe system.

33. M. Barat, J. C. Brenot, D..Dhuicq, J. Pommier, V. Sidis, R. E. Olson, E. J. Shipsey and J. C. Browne, J. Phys. B Atom. Molec. Phys. $\underline{9}$, 269 (1976).

34. H. Helm, J. Phys. B Atom. Molec. Phys. $\underline{9}$, 2931 (1976).

35. S. Sinha and N. Bardsley, Phys. Rev. A $\underline{14}$, 104 (1976).

Fig. 1.   Cross section for producing Xe $6s[3/2]_1^o$ and Xe $6s'[1/2]_1^o$ as

a function of Xe$^+$ + Xe collision energy. Cross sections for

cascading into these levels have been measured as $< 10^{-18}$ cm^2.

Calculation of the cross section assumes that all ^{132}Xe$^+$ ions

present in the beam, formed by 30 V electron impact, react

identically.

Fig. 2.   Upper curve shows the cross section for producing Xe $6s[3/2]_1^o$

in 100 eV (lab) Xe$^+$ + Xe collisions as a function of the electron

ionization voltage used to form the reacting ^{132}Xe$^+$ ions.

Calculation of the cross section takes into account variations

in the ^{132}Xe$^+$ ion flux through the collision chamber. Lower

curve shows the ionization efficiency   for ^{132}Xe$^+$ as

measured at the collision chamber.

Fig. 3.   Lower curve shows the cross section for producing Xe $6s[3/2]_1^o$

as a function of Xe$^+$ + Xe collision energy. Reactant Xe$^+$ ions

are formed using 11.7 V (nominal) electron impact and are assumed

to be predominantly in the ($^2P_{3/2}^o$) state. The upper curve is the

cross section for reaction of Xe$^+$ ($^2P_{1/2}^o$) with xenon to produce

Xe $6s[3/2]_1^o$ as a function of the Xe$^+$ + Xe collision energy. The

cross section is computed from the data in Fig. 1, correcting for

contribution from reaction of Xe$^+$ ($^2P_{3/2}^o$) using the following

assumption based on Amme and Haugsjaa.[6] The ratio of

$^2P_{3/2}^o$: $^2P_{1/2}^o$ in a xenon ion beam formed by 30 V electron impact

is 77 : 23.

71

Fig. 4.   Schematic of mechanism of reaction $Xe^+(^2P^o_{1\,2}) + X(^1S_o) \rightarrow$

$Xe^+ + Xe\ 6s[3/2]^o_1$, showing the relative energy

of the Xe^+_2 system with respect to $Xe^+ (^2P^o_{3/2}) + Xe\ (^1S_o)$ taken

as 0.00 eV. The lower curves (incoming channels) are based on

Wadt's calculations.[31] The dashed curve is an extrapolation of

the incoming channels A and B to higher potential energy and the

upper dotted curves (exit channels) are schematically drawn to

fit the present data. Note that only levels for the lowest

four radiative product channels are depicted.

Xe$^+$ + Xe $\longrightarrow$ Xe$^+$ + Xe$[k]_i^\circ$

Xe$^+$ formed by 30V electron impact

$k = \frac{3}{2}$

$k = \frac{1}{2}$

×4

COLLISION ENERGY , CM (eV)

REACTION CROSS SECTION (10^{-16} cm^2)

73

$Xe^+ + Xe \longrightarrow Xe^+ + Xe\left[^3/_2\right]_1^0$

100 eV collision energy (lab)

ionization efficiency
curve for reactant Xe^+

REACTION CROSS SECTION ($10^{16} cm^2$)

Xe^+ ION CURRENT (nA)

ELECTRON IONIZATION ENERGY (V)

74

$$Xe^+(^2P^\circ_J) + Xe \longrightarrow Xe^+ + Xe[3/2]^\circ_1$$

J = 1/2

J = 3/2

×4

COLLISION ENERGY, CM (eV)

REACTION CROSS SECTION (10^{-16}cm^2)
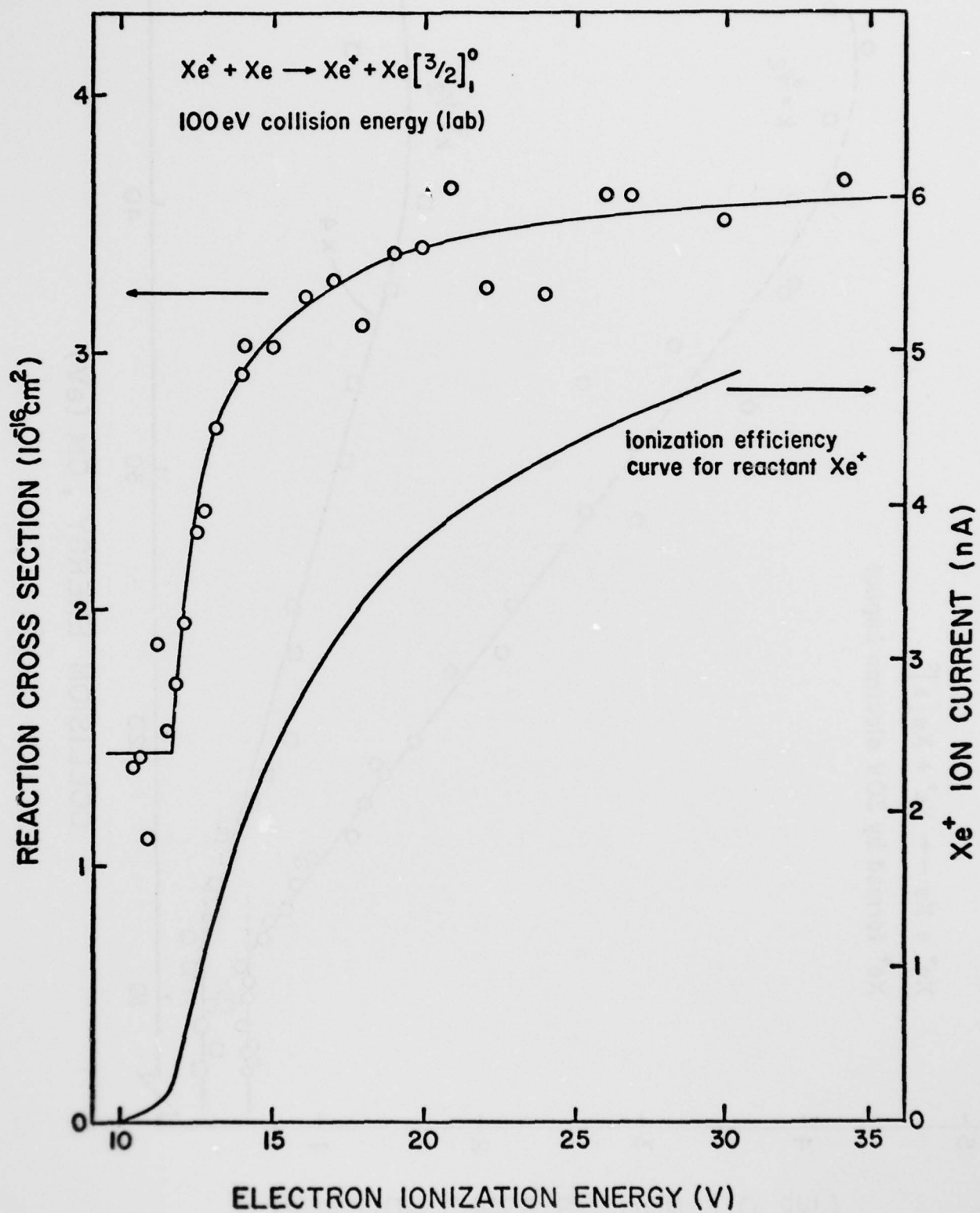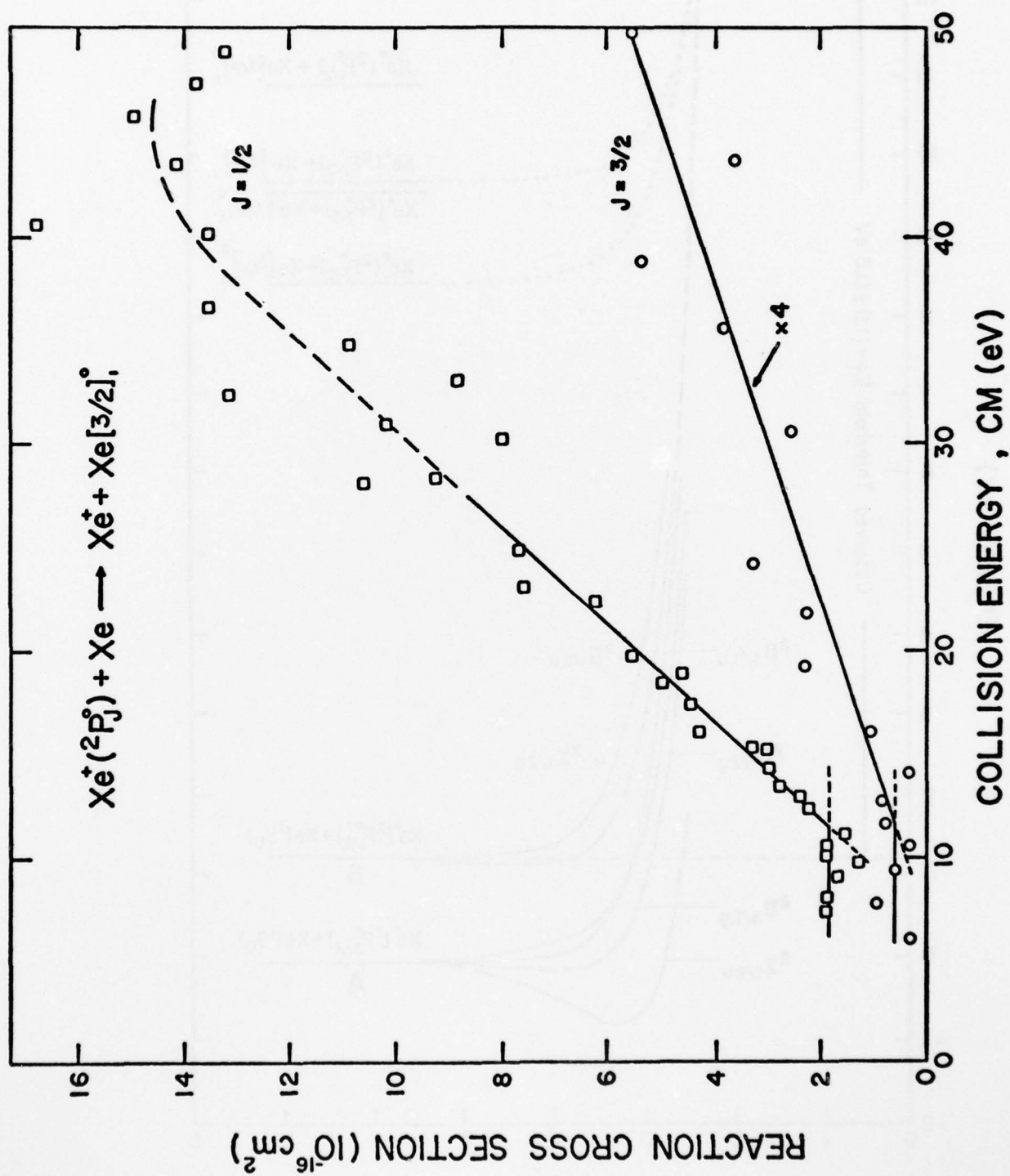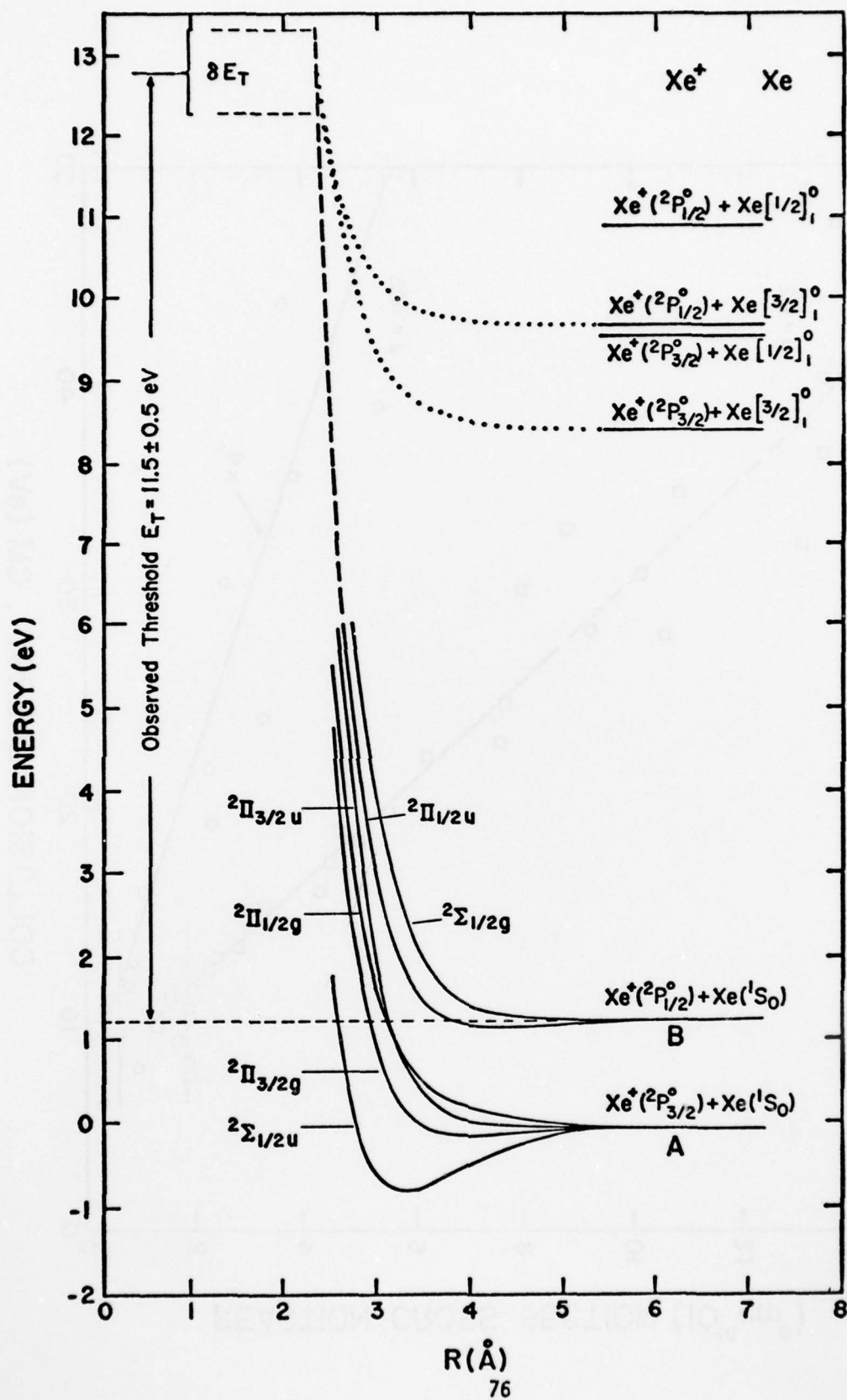
APPENDIX B

PUBLICATIONS AND PRESENTATIONS SUBMITTED DURING COURSE OF CONTRACT

1. E. G. Jones, "Excitation of XeI Resonance Lines in Xe^+/Xe Collisions." Submitted to Phys. Rev.

2. E. G. Jones, B. M. Hughes, T. O. Tiernan, D. C. Fee and D. G. Hopper, "Characterization of the Luminescence from Low Energy He^+/Xe and He^+/Kr Reactions." Spectrochimica Acta - in press.

3. E. G. Jones, T. O. Tiernan, D. C. Fee and B. M. Hughes, "Distribution of Internal Energy in the Products of He^+/Xe Reactions." Submitted to J. Chem. Phys.

4. E. G. Jones, B. M. Hughes, R.L.C. Wu, T. O. Tiernan and D. G. Hopper. Submitted to J. Chem. Phys.

5. E. G. Jones, B. M. Hughes, T. O. Tiernan, D. C. Fee and D. G. Hopper, "Characterization of Luminescence from Low Energy He^+/Xe and He^+/Kr Interactions," Brehm Laboratory Technical Report 10, Wright State University, July 1977.

6. G. D. Sides and E. G. Jones, "Light Emission Produced by Low-Energy Collisions Between He^+ and Fluorine." Presented at the Twenty-Sixth Annual Conference on Mass Spectrometry and Allied Topics, St. Louis, Missouri, May 28-June 2, 1978.

7. D. G. Hopper, E. G. Jones, B. M. Hughes, R.L.C. Wu, and T. O. Tiernan, "Combined Theoretical and Experimental Studies of HeH_2^+ Potential Energy Surfaces Governing Several $He^+ + H_2$ Scattering Processes." Presented at the Twenty-Sixth Annual Conference on Mass Spectrometry and Allied Topics, St. Louis, Missouri, May 28-June 2, 1978.

8. D. G. Hopper, E. G. Jones, R.L.C. Wu, B. M. Hughes and T. O. Tiernan, "Theoretical and Experimental Studies of HeH_2^+ Potential Energy Surfaces for $He^+ + H_2$ Reactions." Presented at the 33rd Symposium on Molecular Spectroscopy at the Ohio State University, Columbus, Ohio, June 12-16, 1978.

9. E. G. Jones, T. O. Tiernan, B. M. Hughes and D. C. Fee, "Distribution of Internal Energy on the Products of Ion-Atom Charge-Transfer Reactions." Presented at the 1978 American Chemical Society Annual Meeting, Miami Beach, Florida, September 10-15, 1978.

10. E. G. Jones, "Electronic Excitation in Xe^+/Xe Collisions." Presented at the 1978 American Chemical Society Annual Meeting, Miami Beach, Florida, September 10-15, 1978.